Cell Reports

Article

Cell-autonomous control of intracellular temperature by unsaturation of phospholipid acyl chains

Graphical abstract

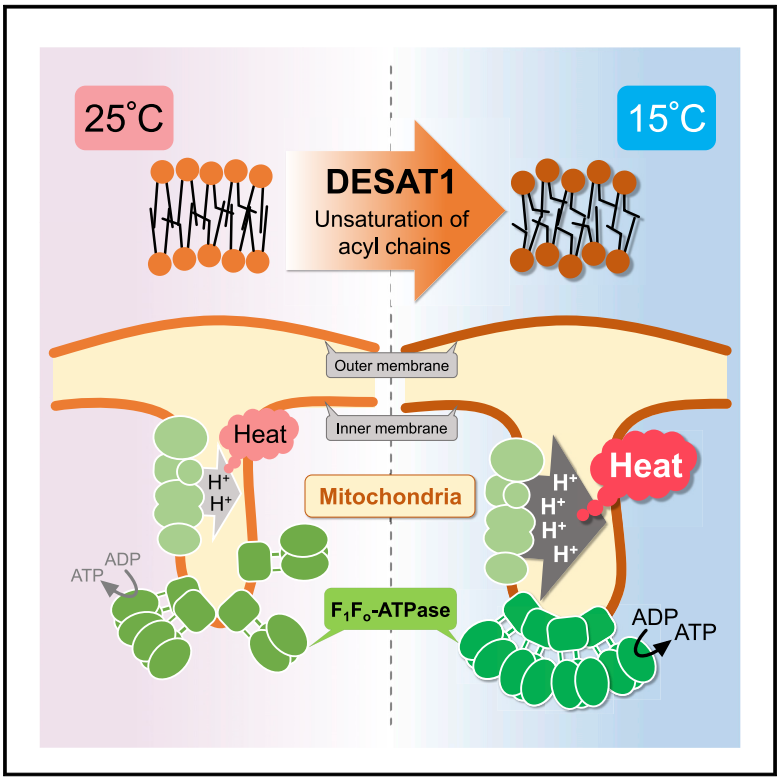

Authors

Akira Murakami, Kohjiro Nagao, Reiko Sakaguchi, ..., Kohki Okabe, Yoshie Harada, Masato Umeda

Correspondence

umeda@sbchem.kyoto-u.ac.jp (M.U.), nagao-k@mb.kyoto-phu.ac.jp (K.N.)

In brief

Murakami et al. show that *Drosophila* S2 cell temperature is maintained by DESAT1-dependent unsaturation of phospholipid acyl chains via modulation of mitochondrial respiration coupled with thermogenesis. Mitochondrial respiration is potentiated upon cold exposure in a DESAT1-dependent manner. We propose a cell-autonomous mechanism for intracellular temperature control in living cells.

Highlights

- *Drosophila* S2 cell temperature is maintained by the Δ9-fatty acid desaturase DESAT1
- DESAT1 upregulates the respiration-dependent heat production in mitochondria
- DESAT1 affects mitochondrial respiration by modulating F_1F_o-ATPase function
- Exposure to cold activates mitochondrial respiration in a DESAT1-dependent manner

Murakami et al., 2022, Cell Reports *38*, 110487
March 15, 2022
https://doi.org/10.1016/j.celrep.2022.110487

CellPress

Cell Reports

CellPress
OPEN ACCESS

Article

Cell-autonomous control of intracellular temperature by unsaturation of phospholipid acyl chains

Akira Murakami,[1,2] Kohjiro Nagao,[1,4,*] Reiko Sakaguchi,[1] Keisuke Kida,[1] Yuji Hara,[1] Yasuo Mori,[1] Kohki Okabe,[2] Yoshie Harada,[3] and Masato Umeda[1,5,6,*]

[1]Department of Synthetic Chemistry and Biological Chemistry, Graduate School of Engineering, Kyoto University, Kyoto 615-8510, Japan
[2]Graduate School of Pharmaceutical Sciences, The University of Tokyo, Tokyo 113-0033, Japan
[3]Institute for Protein Research, Osaka University, Osaka 565-0871, Japan
[4]Present address: Department of Biophysical Chemistry, Kyoto Pharmaceutical University, 5 Misasaginakauchi-cho, Yamashina-ku, Kyoto 607-8414, Japan
[5]Present address: HOLO BIO Co., Ltd, Katsura Innovation Park 1–36, Nishikyo-ku, Kyoto 615–8245, Japan
[6]Lead contact
*Correspondence: umeda@sbchem.kyoto-u.ac.jp (M.U.), nagao-k@mb.kyoto-phu.ac.jp (K.N.)
https://doi.org/10.1016/j.celrep.2022.110487

SUMMARY

Intracellular temperature affects a wide range of cellular functions in living organisms. However, it remains unclear whether temperature in individual animal cells is controlled autonomously as a response to fluctuations in environmental temperature. Using two distinct intracellular thermometers, we find that the intracellular temperature of steady-state *Drosophila* S2 cells is maintained in a manner dependent on Δ9-fatty acid desaturase DESAT1, which introduces a double bond at the Δ9 position of the acyl moiety of acyl-CoA. The DESAT1-mediated increase of intracellular temperature is caused by the enhancement of F_1F_o-ATPase-dependent mitochondrial respiration, which is coupled with thermogenesis. We also reveal that F_1F_o-ATPase-dependent mitochondrial respiration is potentiated by cold exposure through the remodeling of mitochondrial cristae structures via DESAT1-dependent unsaturation of mitochondrial phospholipid acyl chains. Based on these findings, we propose a cell-autonomous mechanism for intracellular temperature control during environmental temperature changes.

INTRODUCTION

As temperature is an important physicochemical parameter that governs biochemical reactions and biomolecular dynamics, intracellular temperature has the potential to influence a broad range of cellular functions (Okabe et al., 2018). Recently developed intracellular thermometers revealed that intracellular temperature is not equal to the extracellular temperature, even in steady-state single cells (Okabe et al., 2012; Sekiguchi et al., 2018). In addition, the temperature within single cells is not homogeneous, as temperature changes occur at a sub-organelle level; temperature fluctuation correlates with cellular functions such as energy metabolism or intracellular Ca^{2+} dynamics (Chretien et al., 2018; Kiyonaka et al., 2013; Kriszt et al., 2017). Thus, it is likely that the spatial and temporal regulation of intracellular temperature is more sophisticated than previously thought. Since changes in the environmental temperature directly affect the intracellular temperature and biological functions of ectotherms, as well as the peripheral tissues in endotherms, the regulation of intracellular temperature during environmental temperature changes is essential for maintaining homeostasis in living cells. However, it remains unclear how individual animal cells autonomously regulate their intracellular temperature in response to environmental temperature changes.

Mitochondria are organelles that have essential functions in a wide range of biological processes, including energy metabolism, Ca^{2+} homeostasis, and signal transduction (Detmer and Chan, 2007). Among these roles, the production of adenosine triphosphate (ATP) via mitochondrial respiration is crucial for energy metabolism. Mitochondria contain two membranes: an outer mitochondrial membrane (OMM) and an inner mitochondrial membrane (IMM) with folded cristae (Formosa and Ryan, 2018). At the IMM, mitochondrial respiratory chain (MRC) complexes I–IV pump protons from the mitochondrial matrix into the intermembrane space, forming a proton gradient across the IMM. Driven by this proton gradient, F_1F_o-ATPase converts adenosine diphosphate (ADP) into ATP. Mitochondria also play an important role in cold adaptation, as the proton gradient can be uncoupled from ATP synthesis to release energy as heat (Cannon and Nedergaard, 2004). Thus, the enhancement of proton leakage by uncoupling proteins that are activated by extracellular stimuli has been known to increase mitochondrial heat production (Boss et al., 1998; Fedorenko et al., 2012). In addition, it is becoming evident that ATP synthesis-coupled

MRC activity also contributes to mitochondrial thermogenesis (Rahbani et al., 2021; Sun et al., 2021). Moreover, recent intracellular thermometry revealed that mitochondria are the main thermogenic organelles even in steady-state cells; the mitochondrial temperature was estimated to be close to 50°C in mammalian cells (Chretien et al., 2018). However, the mechanisms underlying the regulation of mitochondrial thermogenesis and their contributions to the regulation of intracellular temperature remain elusive.

Mitochondrial membrane lipids are important for mitochondrial function, including mitochondrial respiration by MRC complexes (Ikon and Ryan, 2017). Mitochondrial phospholipids are characterized by a high unsaturated fatty acid content in their acyl chains (Hoch, 1992). The amount of unsaturated fatty acids in phospholipid acyl chains affects a broad range of cellular functions via direct binding to proteins or regulation of membrane physicochemical properties, such as membrane fluidity or tension (Hardie, 2007; Holthuis and Menon, 2014). Moreover, because changes in temperature also strongly affect the physicochemical properties of membranes, the regulation of unsaturated fatty acid content in phospholipids is expected to be closely related to responses to temperature changes (Los and Murata, 2004). In particular, the Δ9-fatty acid desaturase (Δ9-desaturase), which introduces a *cis*-double bond at the Δ9 position of saturated acyl-CoA, and is a rate-limiting enzyme for unsaturated fatty acid biosynthesis (Nagao et al., 2019; Ntambi and Miyazaki, 2004), has been thought to be involved in the response to cold by controlling the physicochemical properties of cell membranes (Nakagawa et al., 2002; Tiku et al., 1996). However, it remains unclear whether the regulation of membrane lipid composition is also involved in intracellular temperature control, particularly mitochondrial thermogenesis.

In this study, we investigated the role of membrane lipid biosynthesis in intracellular temperature regulation. We used a series of intracellular thermometry analyses to reveal that DESAT1, the sole Δ9-desaturase in *Drosophila* S2 cells, was responsible for maintaining temperature inside steady-state cells via the upregulation of mitochondrial respiration. Moreover, we identified DESAT1-dependent activation of mitochondrial respiration as a cell-autonomous mechanism for intracellular temperature control during cold exposure. Finally, we discuss the molecular mechanism underlying the regulation of mitochondrial respiration through the production of unsaturated fatty acid-containing phospholipids to maintain intracellular temperature.

RESULTS

Production of unsaturated fatty acids by DESAT1 maintains the intracellular temperature of *Drosophila* S2 cells

To investigate whether the unsaturated fatty acid biosynthesis pathway is involved in intracellular temperature control in *Drosophila* S2 cells, we established a *Desat1*-deficient cell line using the clustered regularly interspaced short palindromic repeats (CRISPR)-Cas9 system (Figures 1A and S1A) (Bassett et al., 2014). Δ9-Desaturase activity was completely abolished in *Desat1*-deficient cells (Figure 1B). *Desat1*-deficient cells displayed auxotrophy for monounsaturated fatty acids, such as palmitoleic acid (C16:1) and oleic acid (C18:1) (Figure S1B), and had to be maintained in medium supplemented with unsaturated fatty acids (50 μM C16:1 and 50 μM C18:1), which reflects the essential role of DESAT1 in S2 cells. When *Desat1*-deficient cells were cultured in a normal medium without unsaturated fatty acid supplementation for 16 h, the amount of monounsaturated fatty acids in the acyl chains of phospholipids decreased, while the saturated fatty acid content increased (Figure 1C). The altered fatty acid composition of phospholipids in *Desat1*-deficient cells was completely rescued by supplementing the culture medium with C16:1 and C18:1 (Figure 1C).

We measured the intracellular temperature of S2 cells using a fluorescent polymeric thermometer (FPT) (Okabe et al., 2012). A cell-permeable FPT (Hayashi et al., 2015) dissolved in 5% glucose/H_2O was spontaneously incorporated into S2 cells within 10 min. The FPT fluorescence lifetime in S2 cells responded to changes in temperature of the culture medium (20°C–30°C) (Figure S1C). The FPT fluorescence lifetime in steady-state S2 cells showed intercellular variations even when a constant culture medium temperature was maintained (Figure S1D). In addition, the intercellular variation in FPT fluorescence lifetime was positively correlated with the mitochondrial membrane potential (Figure S1D). This suggested that the difference in intracellular temperature among cells largely reflects intercellular variations in metabolic activity, such as mitochondrial respiratory activity. As shown in Figure 1D, the FPT fluorescence lifetime was shorter in *Desat1*-deficient cells compared with wild-type cells. The decrease in FPT fluorescence lifetime in *Desat1*-deficient cells was rescued by monounsaturated fatty acid (C16:1 and C18:1) supplementation of the culture medium or exogenous expression of DESAT1-FLAG (Figure 1D), showing that *Desat1* deletion causes the decrease in intracellular temperature. We also analyzed the effect of a chemical DESAT1 inhibitor (SCD1 inhibitor 37c) (Uto et al., 2009) on the intracellular temperature of S2 cells. Incubation of S2 cells with the DESAT1 inhibitor decreased the amount of monounsaturated fatty acids in the acyl chains of phospholipids by approximately 25% (Murakami et al., 2017) and suppressed the cell growth (Figure S1E), which are consistent with the effect of *Desat1* deletion. The FPT fluorescence lifetime significantly decreased after 16 h DESAT1 inhibitor treatment (Figure 1E). Based on the shift in FPT fluorescence lifetime, the estimated temperature change caused by DESAT1 inhibition was about 4°C (Figures 1E and S1C). Reflecting the specificity of the DESAT1 inhibitor, supplementing the culture medium with a monounsaturated fatty acid (C16:1 or C18:1) but not a saturated fatty acid (C16:0) negated the DESAT1 inhibitor-induced decrease in FPT fluorescence lifetime (Figures 1E and S1F). These results revealed that the intracellular temperature of steady-state S2 cells is decreased by DESAT1 deletion or inhibition.

To validate the results obtained in the FPT experiments, we used a genetically encoded green fluorescent protein (GFP)-based thermosensor (tsGFP) (Kiyonaka et al., 2013). In this sensor, the coiled-coil region of the *Salmonella* TlpA undergoes a conformational change in response to temperature changes, which affects the spectral properties of GFP fluorescence. As previously reported, tsGFP1 responds to changes in the temperature at around 37°C, making it unsuitable for the measurement of intracellular temperature of *Drosophila* cells. Therefore, we developed

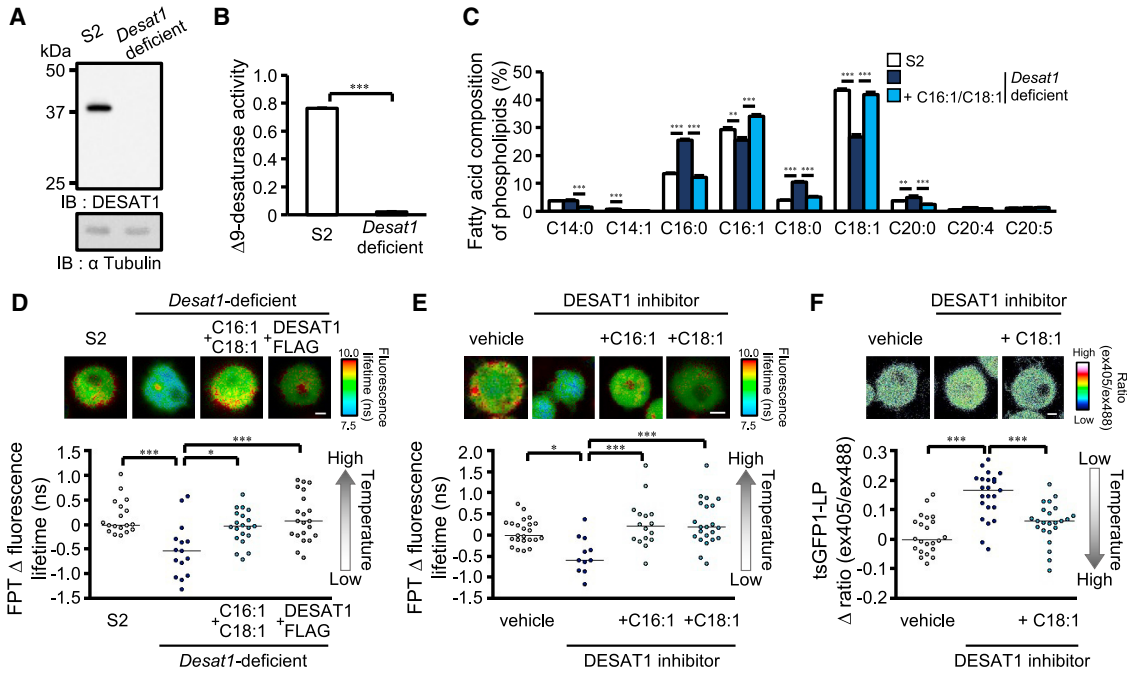

Figure 1. Effect of DESAT1 deletion or inhibition on intracellular temperature

(A) The amount of DESAT1 protein.

(B) The effect of *Desat1* deletion on Δ9-desaturase activity in S2 cells. Mean ± SD (n = 3).

(C) The effect of *Desat1* deletion on the fatty acid composition of cellular phospholipids in S2 cells. Mean ± SD (n = 3).

(D) The effect of *Desat1* deletion on the FPT fluorescence lifetime in S2 cells.

(E) The effect of treatment with the DESAT1 inhibitor (1 μM) for 16 h on the FPT fluorescence lifetime in S2 cells.

(F) The effect of treatment with the DESAT1 inhibitor (1 μM) for 16 h on the ex405/ex488 ratio of tsGFP1-LP in S2 cells.

The average value in each cell was plotted (D–F). The medians are shown as lines (D–F). *p < 0.05, **p < 0.01, ***p < 0.001. Scale bar, 2 μm.

a tsGFP1-LP variant by introducing two proline mutations (L137P in both the TlpA domains) in tsGFP1 (Figure S2A). These mutations destabilize the coiled-coil structure, and thus lower the temperature sensitivity range (Figures S2B and S2C). The fluorescence intensity ratio of the excitation peaks at wavelengths of 392 and 472 nm (ex392/ex472) of the recombinant tsGFP1-LP protein exhibited a sensitive response to a temperature change from 20°C to 30°C. The critical temperature, obtained as the midpoint of the temperature-dependent fluorescence change from the curve (Figure S2), was 25.5°C, which is 12.1°C lower than that of tsGFP1. When tsGFP1-LP was expressed in S2 cells, it showed responsiveness to changes in temperature of the culture medium (20°C–30°C) (Figure S2D). Consistent with the results of the FPT analysis, the ex405/ex488 ratio of tsGFP1-LP increased after treatment with the DESAT1 inhibitor (Figure 1F). These results demonstrate that the intracellular temperature of S2 cells is maintained in a manner dependent on DESAT1-mediated production of unsaturated fatty acids.

DESAT1 regulates MRC activity-dependent thermogenesis in mitochondria

MRC activity has been reported to strongly contribute to intracellular thermogenesis (Chretien et al., 2018; Inomata et al., 2016; Kriszt et al., 2017). As shown in Figure 2A, the ex405/ex488 ratio of tsGFP1-LP in S2 cells increased after inhibition of MRC complex I by rotenone, demonstrating a significant contribution of MRC activity to intracellular temperature control in S2 cells. In contrast, rotenone treatment of DESAT1 inhibitor-treated cells did not further increase the ex405/ex488 ratio of tsGFP1-LP (Figure 2A), suggesting that DESAT1 inhibition affects intracellular temperature in an MRC activity-dependent manner.

The advantage of using a protein-based sensor is that it can easily and specifically be targeted to an organelle by fusing an appropriate targeting signal (VanEngelenburg and Palmer, 2008). A targeting signal from COXVIII was fused to tsGFP1-LP to produce tsGFP1-LP-mito. Confocal images revealed colocalization of tsGFP1-LP-mito with MitoTracker Deep Red, a mitochondrial marker (Figure S2E). Similar to tsGFP1-LP, tsGFP1-LP-mito responded to changes in culture medium temperature (20°C–30°C) (Figure S2F). The ex405/ex488 ratio of tsGFP1-LP-mito increased after rotenone treatment, showing that mitochondrial heat production is dependent on MRC activity in S2 cells (Figure 2B). Similar to rotenone treatment, the DESAT1 inhibitor increased the ex405/ex488 ratio of tsGFP1-LP-mito, while C18:1 supplementation of the culture medium completely negated an increase in the ex405/ex488 ratio of tsGFP1-LP-mito (Figure 2C). In contrast, overexpression of FLAG-DESAT1, which is a calpain-mediated degradation-resistant DESAT1 protein (Murakami et al., 2017), decreased the ex405/ex488 ratio of tsGFP1-LP-mito (Figure 2D), indicating that enhanced unsaturated fatty acid biosynthesis increases the mitochondrial temperature in S2 cells. These intracellular temperature measurements revealed that

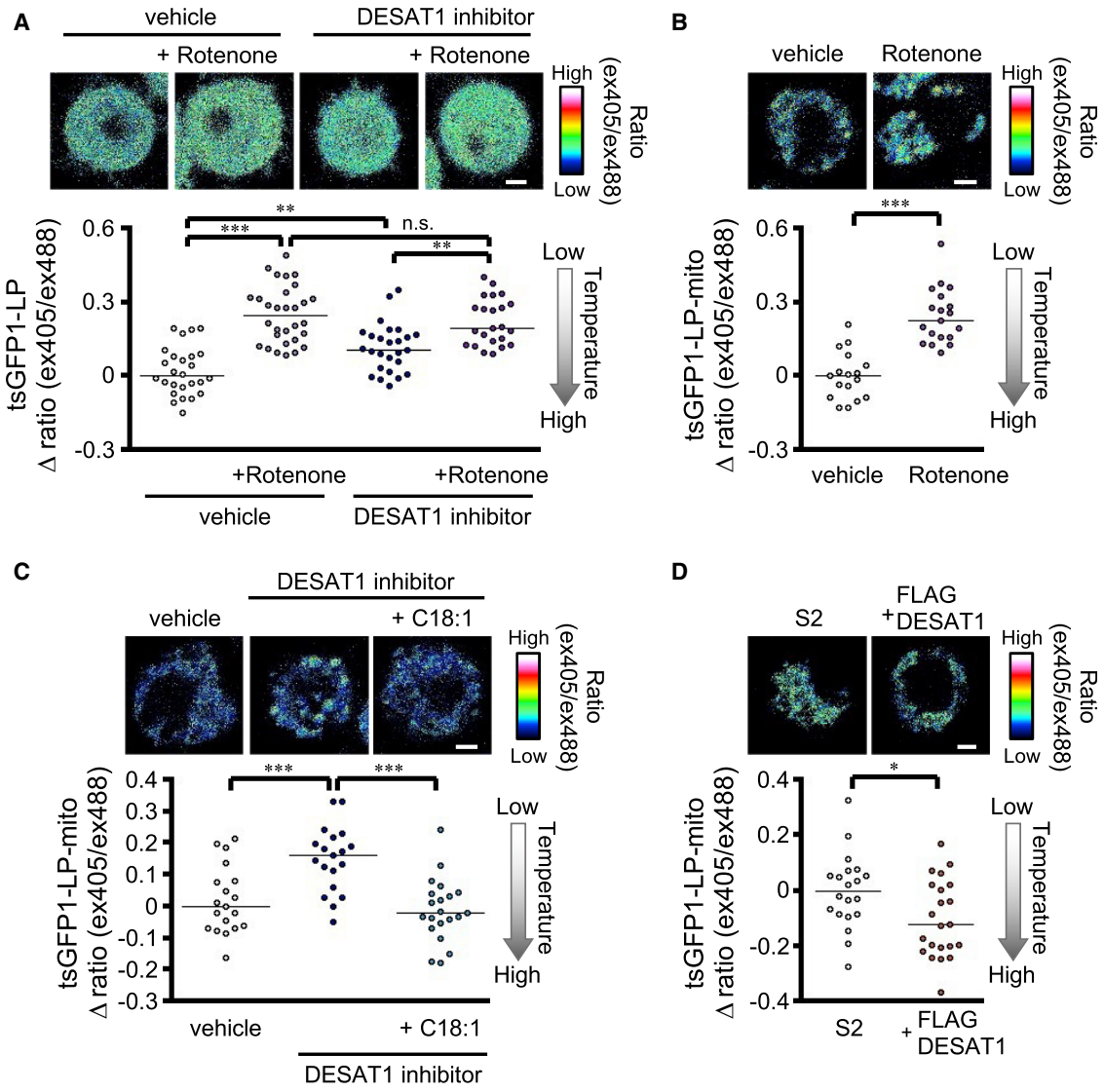

Figure 2. Regulation of MRC activity-dependent thermogenesis in mitochondria by DESAT1

(A) The effect of rotenone on the ex405/ex488 ratio of tsGFP1-LP. S2 cells expressing tsGFP1-LP were incubated with or without the DESAT1 inhibitor (1 μM) for 16 h. Then, the cells were treated with rotenone (5 μM) for 30 min.

(B) The effect of rotenone treatment (5 μM) for 30 min on the ex405/ex488 ratio of tsGFP1-LP-mito in S2 cells.

(C) The effect of treatment with the DESAT1 inhibitor (1 μM) for 16 h on the ex405/ex488 ratio of tsGFP1-LP-mito in S2 cells.

(D) The effect of FLAG-DESAT1 overexpression on the ex405/ex488 ratio of tsGFP1-LP-mito in S2 cells. The Δ ratio was calculated as described in the STAR Methods.

The average value in each cell was plotted. The medians are shown as lines. *$p < 0.05$, **$p < 0.01$, ***$p < 0.001$; n.s., not significant. Scale bar, 2 μm.

unsaturated fatty acid production mediated by DESAT1 is involved in the regulation of MRC activity-dependent thermogenesis in mitochondria.

DESAT1 is involved in the regulation of MRC activity

Given that the MRC activity is coupled to mitochondrial thermogenesis, we examined the contribution of DESAT1 to the regulation of MRC activity. We analyzed mitochondrial membrane potential as an index of MRC activity using JC-1, a small molecule sensitive to the mitochondrial membrane potential (Smiley et al., 1991). Reflecting the requirement of MRC activity in the proton gradient formation in IMM, rotenone treatment caused a significant decrease in mitochondrial membrane potential, while the protonophore FCCP (carbonyl cyanide *p*-(trifluoromethoxy) phenylhydrazone) almost completely abolished the mitochondrial membrane potential in S2 cells (Figure S3A). The mitochondrial membrane potential was decreased by the DESAT1 inhibitor, while C18:1 supplementation of the culture medium completely negated the DESAT1 inhibitor-induced decrease in the mitochondrial membrane potential (Figure 3A). In *Desat1*-deficient

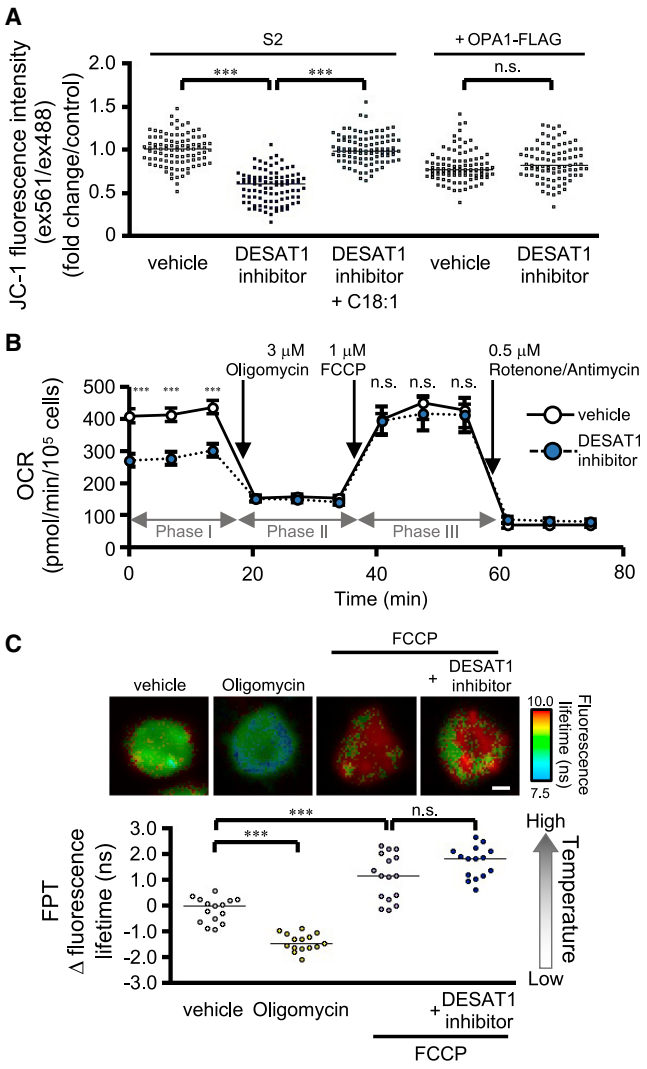

Figure 3. Regulation of ATP synthesis-dependent mitochondrial respiration by DESAT1

(A) The effect of treatment with the DESAT1 inhibitor (1 μM) for 16 h on mitochondrial membrane potential evaluated by JC-1.

(B) The effect of treatment with the DESAT1 inhibitor (1 μM) for 16 h on the oxygen consumption rate (OCR). Mean ± SEM (n = 7).

(C) The effect of treatment with oligomycin or FCCP on FPT fluorescence lifetime in S2 cells. After S2 cells were treated with or without the DESAT1 inhibitor (1 μM) for 16 h, FPT was incorporated into cells and the cells were then incubated with oligomycin (3 μM) for 30 min or FCCP (5 μM) for 15 min.

The average value in each cell was plotted (A and C). The medians are shown as lines (A and C). ***p < 0.001; n.s., not significant. Scale bar, 2 μm.

cells, the decrease in mitochondrial membrane potential was also observed, and this could be rescued by supplementation with unsaturated fatty acids (Figure S3C). In contrast, overexpression of FLAG-DESAT1 in S2 cells increased the mitochondrial membrane potential (Figure S3D). Since the DESAT1 inhibitor did not appear to alter the amount of mitochondrial DNA and mitochondria-localized SESB protein (Figures S3F and S3G), it is likely that DESAT1 is involved in the regulation of MRC activity without affecting mitochondrial content.

DESAT1 enhances ATP synthesis-dependent mitochondrial respiration

To understand how DESAT1 regulates MRC activity, we analyzed the oxygen consumption rate (OCR), which directly describes the level of cellular respiratory activity. Most of the OCR in S2 cells was found to be MRC activity-dependent (rotenone/antimycin-sensitive) (Figure 3B), indicating that the OCR in S2 cells largely reflects the mitochondrial respiratory activity level.

As shown in Figure 3B, the DESAT1 inhibitor decreased the mitochondrial basal OCR (phase I). In addition, the basal OCR in *Desat1*-deficient cells was lower than that in wild-type S2 cells (Figure S3I), indicating that DESAT1 deletion or inhibition suppresses steady-state mitochondrial respiratory activity. Because the inhibition of mitochondrial respiration by rotenone decreases the cellular and mitochondrial temperature (Figures 2A and 2B), a decrease in intracellular temperature of *Desat1*-deficient and DESAT1 inhibitor-treated cells is likely caused by decreased mitochondrial respiratory activity. However, ATP synthesis-independent OCR (oligomycin-insensitive OCR) (phase II) and maximum OCR (FCCP-induced OCR) (phase III) were not affected by the DESAT1 deletion or inhibition (Figures 3B and S3I). In addition, the DESAT1 inhibitor did not affect the levels of MRC complex proteins (Figure S3H). These results indicate that DESAT1 inhibition does not affect the electron transfer capacities of MRC complexes I–IV. Reflecting an intact electron transfer capacity, DESAT1 deletion or inhibition did not suppress the increase in FPT fluorescence lifetime caused by FCCP treatment (Figures 3C and S3K).

On the other hand, DESAT1 deletion or inhibition caused a decrease in ATP synthesis-dependent OCR (oligomycin-sensitive OCR) (Figures 3B and S3I). While the 5-min inhibition of F_1F_o-ATPase by oligomycin treatment transiently increased the mitochondrial membrane potential, evaluated by JC-1 and TMRM, the 30-min oligomycin treatment decreased the mitochondrial membrane potential (Figures S3A and S3B). This indicates that ATP synthesis-dependent mitochondrial respiratory activity is essential for maintaining mitochondrial membrane potential in S2 cells. In addition, 30 min of oligomycin treatment decreased the intracellular temperature in S2 cells (Figure 3C), indicating that appropriate ATP synthesis-dependent mitochondrial respiratory activity is required for intracellular temperature maintenance. Thus, it was suggested that DESAT1 is involved in the control of intracellular temperature via regulation of ATP synthesis-dependent mitochondrial respiration in S2 cells.

DESAT1 modulates F_1F_o-ATPase activity via regulation of the IMM structure

To examine the mechanism underlying DESAT1-dependent regulation of ATP synthesis-dependent mitochondrial respiration, we analyzed the enzymatic activity of F_1F_o-ATPase. The DESAT1 inhibitor decreased F_1F_o-ATPase activity by 54%, and C18:1 supplementation of the culture medium rescued F_1F_o-ATPase activity (Figure 4A). As the activity of F_1F_o-ATPase is regulated by its oligomerization (Arselin et al., 2004), we evaluated the oligomerization of F_1F_o-ATPase by analyzing the high-molecular-weight complex formation of ATP5A, a subunit of the F_1 domain in F_1F_o-ATPase. The blue native polyacrylamide gel electrophoresis (BN-PAGE) analysis revealed that the

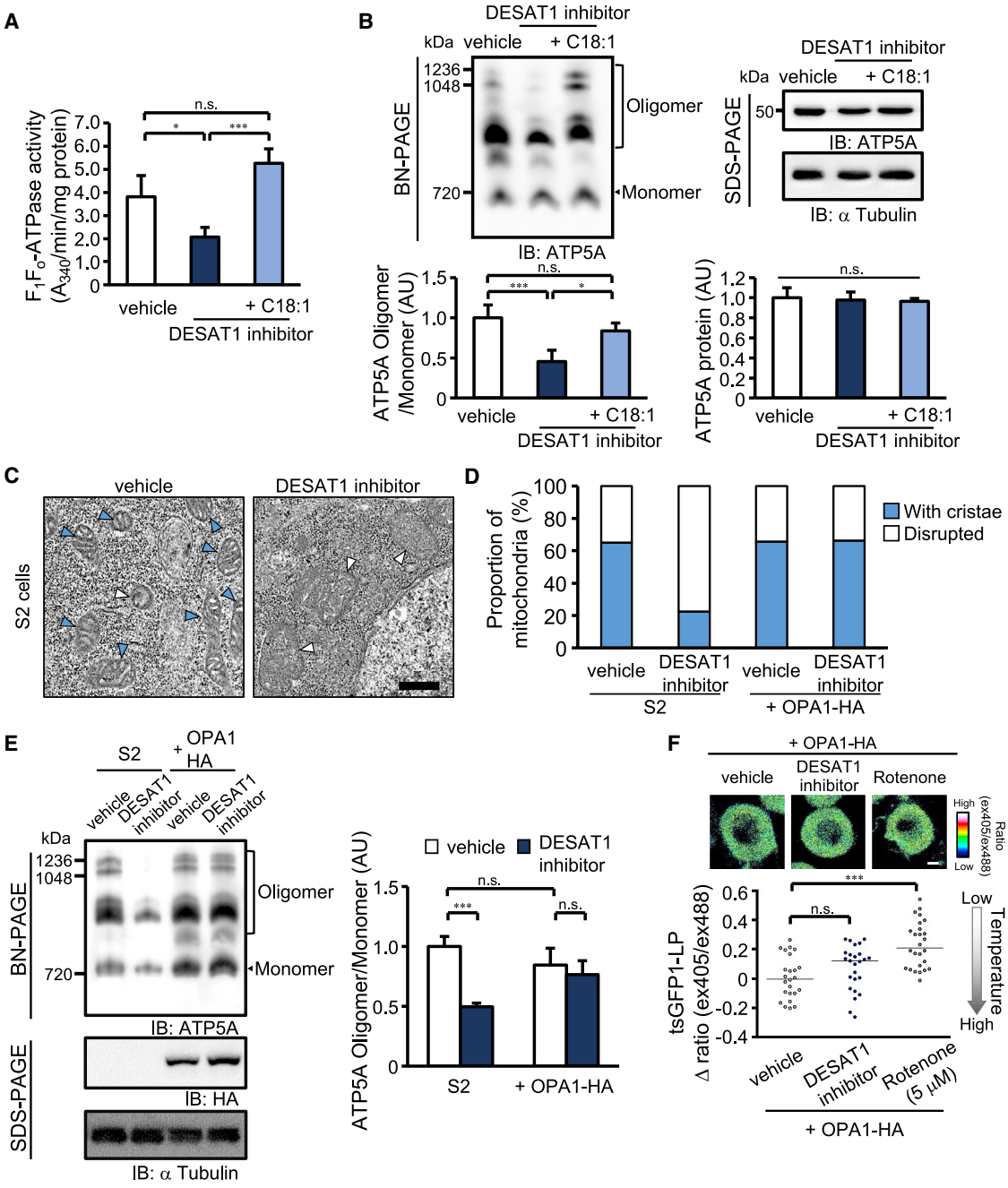

Figure 4. DESAT1-dependent regulation of F_1F_o-ATPase activity via control of cristae structure

(A) The effect of treatment with the DESAT1 inhibitor (1 μM) for 16 h on F_1F_o-ATPase activity. Mean ± SD (n = 3).

(B) The effect of treatment with the DESAT1 inhibitor (1 μM) for 16 h on the oligomerization of F_1F_o-ATPase. The levels of F_1F_o-ATPase oligomer are shown relative to the amount of F_1F_o-ATPase monomer. The amount of ATP5A protein was normalized with that of α-tubulin. Mean ± SD (n = 3).

(C) Mitochondrial structure of S2 cells observed in transmission electron microscopy. Most mitochondria in S2 cells showed "with cristae" structure (blue arrow head), while mitochondria with "disrupted" structure were also observed especially in DESAT1 inhibitor-treated cells (white arrow head). Scale bar, 500 nm.

(D) The effect of treatment with the DESAT1 inhibitor (1 μM) for 16 h on the mitochondrial structure. The proportions of mitochondria classified as in (C) in vehicle-treated S2 cells (n = 214), DESAT1 inhibitor-treated S2 cells (n = 106), vehicle-treated OPA1-HA-overexpressing S2 cells (n = 149), and DESAT1 inhibitor-treated OPA1-HA-overexpressing S2 cells (n = 125).

(E) The effect of OPA1 overexpression on the oligomerization of F_1F_o-ATPase. Mean ± SD (n = 3).

(F) The effect of treatment with the DESAT1 inhibitor (1 μM) for 16 h on the ex405/ex488 ratio of tsGFP1-LP in OPA1-HA-overexpressing S2 cells. Scale bar, 2 μm. The average value in each cell was calculated. The medians are shown as lines. *p < 0.05, ***p < 0.001; n.s., not significant.

DESAT1 inhibitor caused a 2.2-fold decrease in the proportion of ATP5A present in the high-molecular-weight complexes, which was negated by C18:1 culture supplementation (Figure 4B). This indicates that F_1F_o-ATPase oligomers are disrupted by DESAT1 inhibition. In contrast, sodium dodecyl sulfate-polyacrylamide gel electrophoresis (SDS-PAGE) analysis showed that the DESAT1 inhibitor did not affect the total amount of ATP5A (Figure 4B), suggesting that the amount of F_1F_o-ATPase is not changed by DESAT1 inhibition. The impaired formation of the F_1F_o-ATPase oligomers was also observed in *Desat1*-deficient cells cultured in a normal medium without C16:1 and C18:1 supplementation (Figure S4A), whereas overexpression of FLAG-DESAT1 in the wild-type cells increased the proportion of the oligomerized F_1F_o-ATPase (Figure S4C). These results indicate that DESAT1 regulates the structure and activity of F_1F_o-ATPase, which is critical for the upregulation of intracellular temperature via mitochondrial thermogenesis.

Because appropriate mitochondrial structure is reportedly required for F_1F_o-ATPase oligomerization and activity (Rabl et al., 2009), we analyzed the mitochondrial structure in S2 cells by transmission electron microscopy. Similar to a previous observation (Abdelwahid et al., 2007), most mitochondria in S2 cells showed elongated morphology with a dense matrix and well-ordered cristae (“with cristae”); however, swelled mitochondria with a rounder shape, less dense matrix, and abnormal cristae (“disrupted”) were also observed (Figure 4C). As shown in Figure 4D, DESAT1 inhibitor treatment decreased the proportion of “with cristae” mitochondria. Consistent with this, the proportion of “with cristae” mitochondria was decreased in *Desat1*-deficient cells (Figure S4B). In contrast, overexpression of FLAG-DESAT1 increased the proportion of “with cristae” mitochondria (Figure S4D). These results suggested that DESAT1 regulates F_1F_o-ATPase via control of the IMM structure. To investigate the role of the IMM structure control in DESAT1-mediated regulation of mitochondrial respiratory activity, we evaluated the effect of the overexpression of OPA1, an IMM fusion factor (Civiletto et al., 2015; Varanita et al., 2015). As shown in Figure 4D, overexpression of OPA1 reversed the DESAT1 inhibitor-induced decrease in the proportion of “with cristae” mitochondria. The OPA1-dependent remodeling of the cristae structure rescued the DESAT1 inhibitor-induced mitochondria membrane potential decline (Figure 3A) and disruption of F_1F_o-ATPase oligomers (Figure 4E). Moreover, the DESAT1 inhibitor-induced decrease in intracellular temperature evaluated by tsGFP1-LP was also rescued by OPA1 overexpression (Figure 4F). As the expression level of OPA1 was not affected by DESAT1 inhibition (Figure S4E), the defect in cristae formation was not caused by the aberrant expression of OPA1 in DESAT1-suppressed cells. These results reveal that DESAT1 controls the intracellular temperature of steady-state S2 cells through regulating the IMM-localized F_1F_o-ATPase via control of cristae structure.

Regulation of mitochondrial lipids by endoplasmic reticulum-localized DESAT1

We examined the contribution of DESAT1 to the regulation of mitochondrial membrane lipids because DESAT1 is a Δ9-desaturase that produces monounsaturated fatty acids. Consistent with the reported localization of Δ9-desaturase proteins in mammals and yeast (Kato et al., 2006; Tatzer et al., 2002), C-terminally HA-tagged DESAT1 (DESAT1-HA) was co-localized with the ER marker (Bip-GFP-KDEL) (Figure 5A). Although apparent colocalization was not observed, DESAT1-HA was adjacent to mitochondria (Mito-EGFP) (Figure 5B). In addition, biochemical organelle fractionation revealed that DESAT1 was detected in the crude mitochondrial fraction rather than the ER fraction (Figure 5C).

To reveal the role of DESAT1 in the regulation of mitochondrial membrane lipids, LC-ESI-MS analysis of the crude mitochondrial fraction was performed. The contents of unsaturated fatty acid-containing phosphatidylcholine (PC) and phosphatidylethanolamine (PE) species in the crude mitochondria were found to be markedly altered by treatment with the DESAT1 inhibitor for 16 h (Figures 5D and 5E). In particular, the amounts of PC molecules containing two monounsaturated fatty acids, such as PC (32:2), PC (34:2), and PC (36:2) were decreased by 10-, 10-, and 6.3-fold through DESAT1 inhibition, respectively (Figures 5D and S5A–S5C). The amounts of PE molecules with two monounsaturated fatty acids, such as PE (32:2), PE (34:2), and PE (36:2), were also reduced by 52%, 46%, and 44% through treatment with the DESAT1 inhibitor, respectively (Figures 5E and S5D–S5F). Major cardiolipin (CL) molecules in S2 cells were CL (64:4), CL (66:4), and CL (68:4), which consist of four monounsaturated fatty acids (Figures S5G–S5J). Similar to PC and PE molecules with two unsaturated fatty acids, the amount of CL (64:4) was decreased by DESAT1 inhibition, while DESAT1 inhibition caused increases in the amounts of CL (66:4) and CL (68:4) (Figure 5F), illuminating the complex regulatory mechanism for the modulation of CL acyl chains. DESAT1 is the sole Δ9-desaturase in S2 cells (Murakami et al., 2017) and is localized adjacent to the mitochondria (Figures 5B and 5C). Moreover, the defects of mitochondrial functions in DESAT1 inhibitor-treated or *Desat1*-deficient cells were rescued by supplementation with unsaturated fatty acids. Thus, it is apparent that DESAT1 regulates mitochondrial functions by modulating the contents of unsaturated fatty acid-containing phospholipids in mitochondria.

DESAT1-dependent increase in unsaturation of phospholipid acyl chains and activation of F_1F_o-ATPase-dependent mitochondrial respiration during cold exposure

It has been reported that the amount of unsaturated fatty acids in acyl chain of phospholipids is increased in response to cold exposure in order to maintain the physicochemical properties and biological functions of cell membranes (Tiku et al., 1996). Since DESAT1 overexpression increased the mitochondrial membrane potential and the mitochondrial thermogenesis (Figures 2D and S3D), we hypothesized that the F_1F_o-ATPase-dependent mitochondrial respiration could be potentiated by the enhanced production of unsaturated fatty acids as a cell-autonomous response to cold exposure.

S2 cells were incubated for 4 h at 15°C, which is 10°C lower than normal culture conditions. Although an apparent change in the expression level of DESAT1 protein was not observed (Figure S6A), the proportion of C16:1 in phospholipid acyl chains increased upon cold exposure in a DESAT1-dependent manner

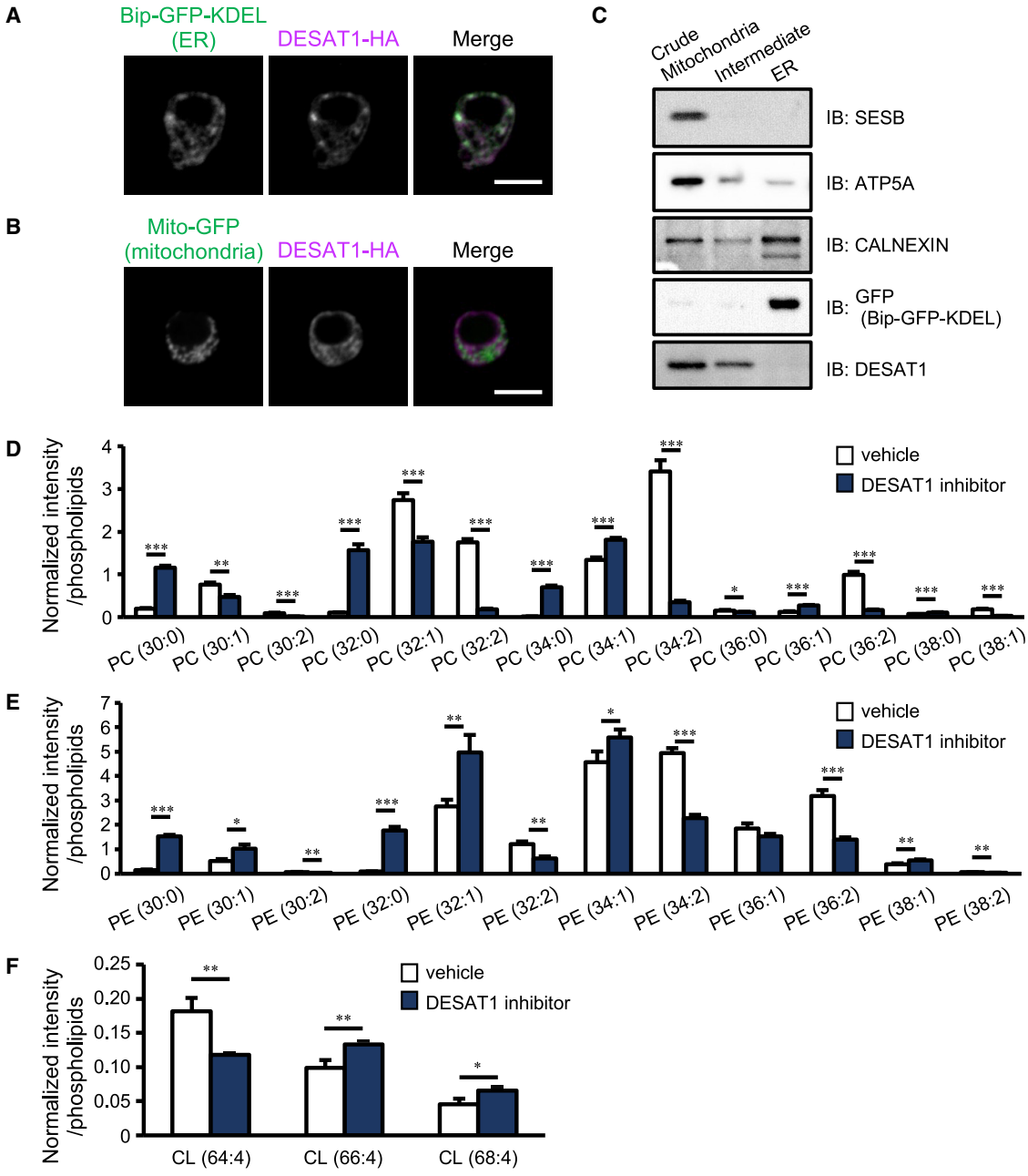

Figure 5. Regulation of mitochondrial lipids by endoplasmic reticulum-localized DESAT1 intracellular localization of DESAT1 protein observed using confocal microscopy

(A and B) Bip-GFP-KDEL (A) or Mito-EGFP (B) was exogenously expressed in *Desat1*-deficient cells expressing DESAT1-HA. DESAT1-HA was visualized using anti-HA antibody. Scale bar, 5 μm.

(C) Organelle fractionation of S2 cells. SESB protein is an inner mitochondrial protein. ATP5A protein is a component of the F1 subunit of inner mitochondrial F_1F_o-ATPase. Calnexin is an ER membrane protein. Bip-GFP-KDEL is a GFP protein fused with ER localization signals. PC (D), PE (E), and CL (F) molecules of the crude mitochondrial fraction in S2 cells treated with vehicle or the DESAT1 inhibitor (1 μM) for 16 h were analyzed using liquid chromatography-tandem mass spectroscopy (LC-MS/MS). Phospholipid molecules were presented in the format PC (X:Y), PE (X:Y), and CL (X:Y), where X denotes the total number of acyl chain carbons and Y denotes the total number of double bonds in acyl chains. Values are mean ± SD (n = 3). *p < 0.05, **p < 0.01, ***p < 0.001.

(Figure 6A). The amounts of mitochondrial phospholipid species with two monounsaturated fatty acids, such as PC (32:2), PC (34:2), and PE (32:2) were significantly increased by cold exposure (Figures 6B, 6C, and S6B–S6D). The amount of PE (34:2), a major PE molecule with two monounsaturated fatty acids, and the composition of CL in mitochondria, were not significantly changed by cold exposure in S2 cells (Figures 6C, S6E, and S6F). This may reflect that DESAT1 has a stronger contribution

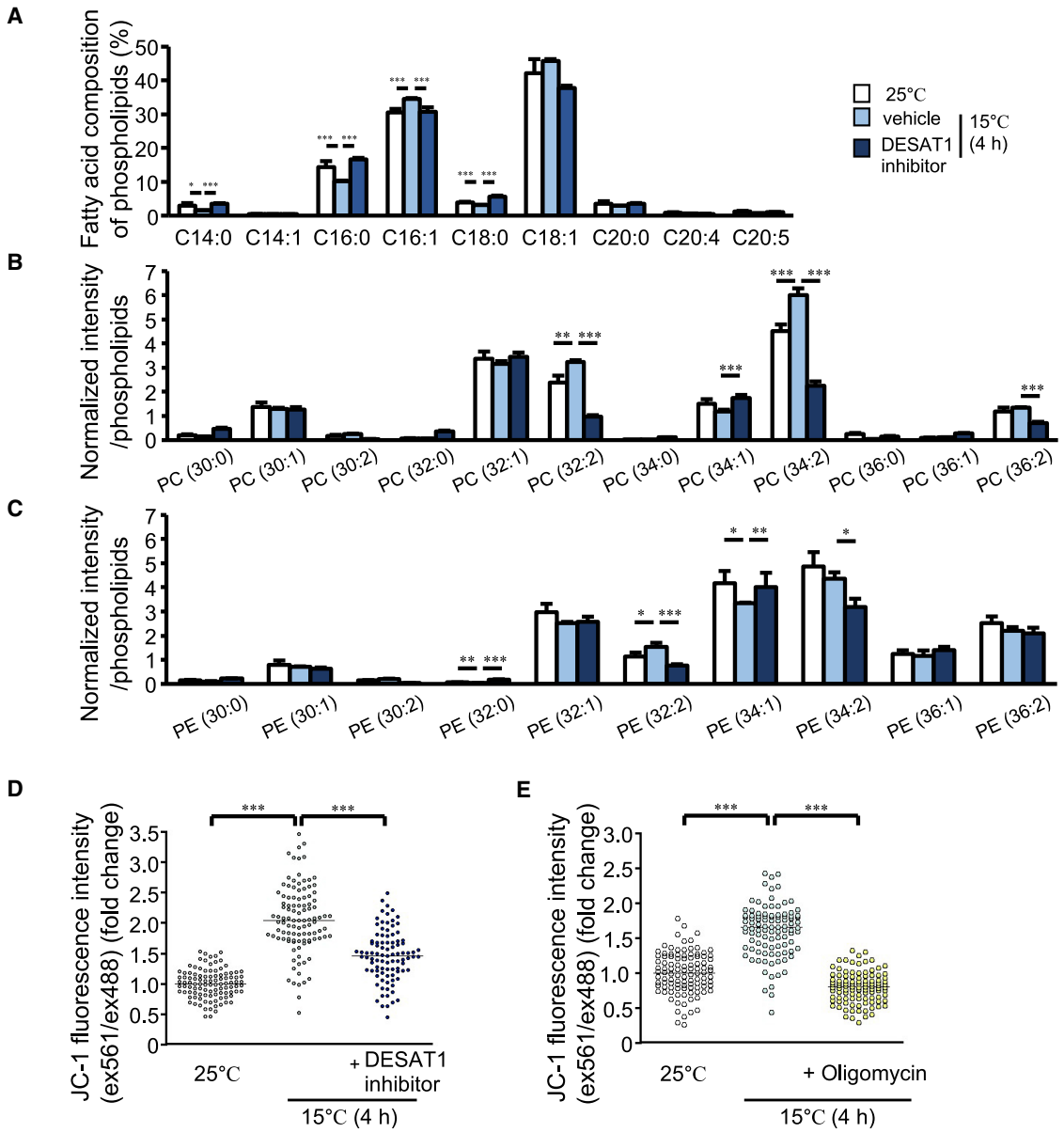

Figure 6. DESAT1-dependent enhancement of mitochondrial respiratory activity during acute cold exposure

(A) The effect of 15°C exposure for 4 h on the fatty acid composition of cellular phospholipids in S2 cells. Mean ± SD (n = 3).

(B and C) The effect of 15°C exposure for 4 h on the composition of mitochondrial phospholipid species. PC (B) and PE (C) molecules of the crude mitochondrial fraction in S2 cells treated with or without the DESAT1 inhibitor (1 μM) for 4 h at 15°C or 25°C were analyzed using LC-MS/MS. Phospholipid molecules were presented in the format PC (X:Y) and PE (X:Y), where X denotes the total number of acyl chain carbons and Y denotes the total number of double bonds in acyl chains. Values are mean ± SD (n = 3).

(D) The effect of 15°C exposure for 4 h on mitochondrial membrane potential evaluated by JC-1.

(E) The effect of F_1F_o-ATPase inhibition on the increase in mitochondrial membrane potential during cold exposure. The S2 cells were cultured in the culture medium with or without oligomycin (3 μM) at 15°C for 4 h. The mitochondrial membrane potential was evaluated using JC-1. The average value in each cell was plotted (D and E). The medians are shown as lines (D and E). *p < 0.05, **p < 0.01, ***p < 0.001.

to the regulation of mitochondrial membrane PC than PE or CL at normal temperatures (Figures 5D–5F). These results demonstrate that DESAT1-mediated unsaturation of mitochondrial membrane lipids is upregulated during cold exposure in S2 cells.

Similar to the effect of DESAT1 overexpression (Figure S3D), the mitochondrial membrane potential in S2 cells was increased 2-fold upon cold exposure (Figure 6D). The cold-induced increase in mitochondrial membrane potential was significantly suppressed in DESAT1 inhibitor-treated and *Desat1*-deficient cells (Figures 6D and S6G). Levels of mitochondrial proteins SESB and ATP5A did not increase during incubation of S2 cells at 15°C for 4 h (Figures S6H and 7B), indicating that the observed

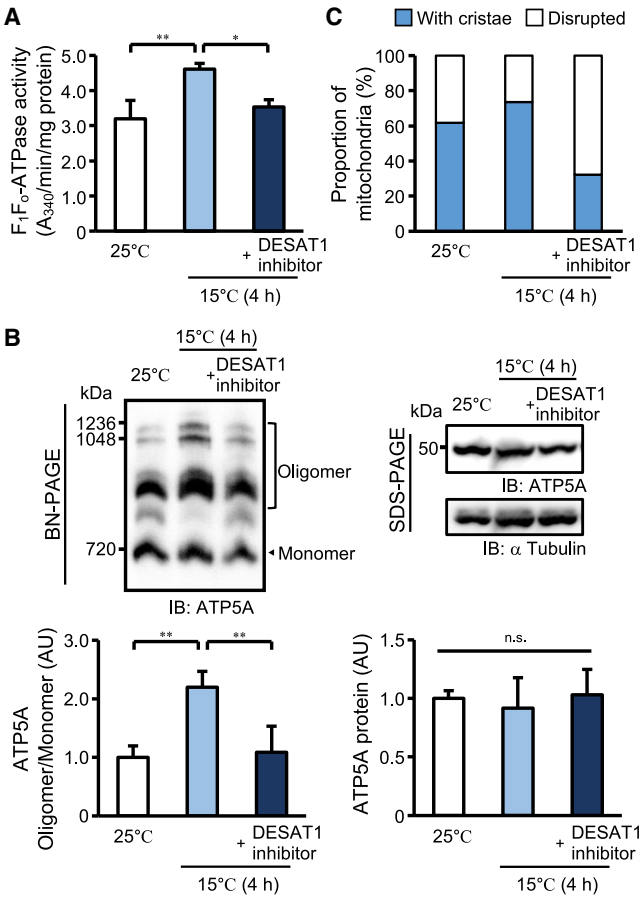

Figure 7. Cold-induced activation of F_1F_o-ATPase through the DESAT1-dependent cristae remodeling

(A) The effect of 15°C exposure for 4 h on F_1F_o-ATPase activity. Mean ± SD (n = 3).

(B) The effect of 15°C exposure for 4 h on the oligomerization of F_1F_o-ATPase. The levels of F_1F_o-ATPase oligomer are shown relative to the amount of F_1F_o-ATPase monomer. The amount of ATP5A protein was normalized with that of α-tubulin. Mean ± SD (n = 3).

(C) The effect of 15°C exposure for 4 h on the mitochondrial structure. The proportions of mitochondria classified as Figure 4C in S2 cells cultured at 25°C for 4 h (n = 230), S2 cells cultured at 15°C for 4 h (n = 226), and S2 cells treated with the DESAT1 inhibitor (1 μM) at 15°C for 4 h (n = 96). *p < 0.05, **p < 0.01; n.s., not significant.

increase in mitochondrial membrane potential during cold exposure does not result from increased mitochondrial biogenesis. In addition, the cold-induced membrane potential increase was suppressed by the F_1F_o-ATPase inhibitor oligomycin (Figure 6E), showing that the cold-induced increase in membrane potential was dependent on the F_1F_o-ATPase activity and not caused by a decrease in consumption of the proton gradient. To evaluate the dynamics of proton gradient formation in mitochondria during cold exposure, we analyzed the recovery rate of mitochondrial membrane potential after rotenone treatment. We first found that the recovery of mitochondrial membrane potential was F_1F_o-ATPase activity dependent (oligomycin sensitive) (Figure S6I). Moreover, the recovery rate of the mitochondrial membrane potential increased with cold exposure, which was negated by DESAT1 inhibition (Figure S6J). These results suggested that the increase in mitochondrial membrane potential is caused by the DESAT1-mediated upregulation of F_1F_o-ATPase-dependent proton pumping across IMM during cold exposure.

Activation of F_1F_o-ATPase-dependent mitochondrial respiration via cristae remodeling during cold exposure

To determine the mechanism by which DESAT1 upregulates F_1F_o-ATPase-dependent mitochondrial respiration in cold environments, we first examined the activity and structure of F_1F_o-ATPase at low temperatures. As shown in Figure 7A, the enzymatic activity of F_1F_o-ATPase was found to be increased 1.4-fold. The proportion of oligomerized F_1F_o-ATPase increased 2.2-fold after cold exposure, and this effect was suppressed by the inhibition or deletion of DESAT1 (Figures 7B and S7A). Moreover, the proportion of "with cristae" mitochondria was increased upon cold exposure, while this cristae remodeling was not observed in DESAT1 inhibitor-treated or *Desat1*-deficient cells (Figures 7C and S7B). Taken together, these data demonstrate that the F_1F_o-ATPase-dependent mitochondrial respiration is upregulated by DESAT1-mediated control of F_1F_o-ATPase activity through cristae remodeling during cold exposure. Since F_1F_o-ATPase-dependent mitochondrial respiration is coupled with mitochondrial thermogenesis in S2 cells, these findings reveal a cell-autonomous mechanism for the control of intracellular temperature during environmental temperature changes.

DISCUSSION

Although mitochondrial thermogenesis has long been recognized as essential for cold responses in living organisms, it remains unclear how the temperature in single animal cells is regulated autonomously. In this study, using two distinct intracellular thermometers, we revealed that Δ9-desaturase DESAT1 is involved in the cell-autonomous regulation of intracellular temperature via mitochondrial respiration. Moreover, we found that the DESAT1-dependent mitochondrial respiratory activity is potentiated by cold exposure. Thus, it is likely that the production of unsaturated fatty acid-containing phospholipids during cold exposure is involved not only in the control of the physicochemical properties of cell membranes but also in the enhancement of mitochondrial respiration in response to cold environments.

We found that DESAT1-mediated production of unsaturated fatty acids is required for the appropriate enzymatic activity and oligomerization of F_1F_o-ATPase (Figures 4A and 4B). Since F_1F_o-ATPase is essential for the mitochondrial respiratory activity and intracellular temperature control (Figures 3B and 3C), it is apparent that F_1F_o-ATPase is a crucial effector in DESAT1-dependent regulation of intracellular temperature. We also revealed that DESAT1 is required for the formation of well-ordered IMM cristae structures. The disrupted IMM cristae structure caused by DESAT1 inhibition was rescued by OPA1 overexpression (Figure 4D). Moreover, because OPA1 overexpression also rescued decreases in the mitochondrial membrane potential, the

oligomer formation of F_1F_o-ATPase, and intracellular temperature in DESAT1-suppressed cells (Figures 3A, 4E, and 4F), it is apparent that the remodeling of the IMM cristae structure is upstream of F_1F_o-ATPase regulation in DESAT1-mediated control of intracellular temperature. On the other hand, because inhibition of F_1F_o-ATPase by oligomycin causes disruption of cristae structure (Figure S4F), it is likely that F_1F_o-ATPase regulates the IMM structure in S2 cells, and vice versa. Thus, the activation of F_1F_o-ATPase by DESAT1 may further enhance the cristae remodeling and oligomer formation of F_1F_o-ATPase to accelerate the activity of F_1F_o-ATPase in a feedforward manner. Therefore, DESAT1 is a crucial regulator of F_1F_o-ATPase function that upregulates the intracellular temperature via mitochondrial respiratory activity-dependent thermogenesis.

Previous studies demonstrated that mitochondrial phospholipids are an intrinsic component of mitochondrial respiratory activity. For example, CL and PE molecules are known to be important for proper mitochondrial fusion and the maintenance of the membrane potential (Brandner et al., 2005; Joshi et al., 2012). In addition, CL molecules bind directly to F_1F_o-ATPase, which is essential for the assembly of the F_1F_o-ATPase oligomer (Duncan et al., 2016). Previous reports show that maturated CLs containing linoleic acid (C18:2) are important for mitochondrial functions (Minkler and Hoppel, 2010). In contrast to C18:2-enriched CL molecules in mammalian cells, major CL molecules in S2 cells have four monounsaturated fatty acids (Figures S5G–S5J). Thus, it is likely that C18:2-containing CL molecules are not essential for the mitochondrial respiratory activity in S2 cells. Moreover, S2 cells do not contain C18:2 in the acyl chains of phospholipids due to ineffective uptake of extracellular fatty acids (Matsuo et al., 2019). These observations indicate that S2 cells can *de novo* synthesize the fatty acids required for control of proper mitochondrial function independent of their uptake from the extracellular environment. We also found that DESAT1 modulates the acyl chain composition of PC molecules more efficiently than those of CL and PE molecules (Figures 5D–5F). Recently, a lipidome-wide fluxomic analysis in adult *Drosophila* demonstrated that the turnover rates of PC molecules are faster than those of CL and PE molecules (Schlame et al., 2020). In addition, the fatty acyl chains of CL are known to be modulated by transacylations with the acyl chains of PC molecules (Xu et al., 2006). Thus, the difference in the biosynthesis rate and mechanism of acyl chain exchange of each phospholipid molecule may enable the selective unsaturation of phospholipid acyl chains by DESAT1. The composition of mitochondrial phospholipids is reported to differ between the OMM and the IMM, with the IMM being rich in CL molecules (Paradies et al., 2014). Since DESAT1 inhibition influenced the acyl chain compositions of PC and PE molecules as well as CL molecules (Figures 5D–5F), it is likely that DESAT1 is involved in regulating the phospholipid compositions of the cristae-forming IMM in which MRC complexes, such as F_1F_o-ATPase, localize. We also showed that ER-embedded DESAT1 localizes near the mitochondria (Figures 5A–5C). The contact site between the ER and mitochondria is also known as the mitochondria-associated membrane (Vance, 1990), and was originally proposed to be an important hub for phospholipid biosynthesis. In addition, supplementing the culture medium with a monounsaturated fatty acid did not increase the mitochondrial membrane potential or OCR in control cells (Figures S3E and S3J). It is therefore assumed that DESAT1 is localized at the contact site between the ER and mitochondria to efficiently supply the unsaturated fatty acids to the mitochondria. Thus, it is apparent that DESAT1-mediated unsaturated fatty acid synthesis is suitable for cell-autonomous regulation of mitochondrial respiratory activity to control the intracellular temperature.

The increase in mitochondrial respiration represents an important function in cold adaptation via a compensation for decrease in intracellular temperature. However, the mechanisms and physiological role of mitochondria thermogenesis are mainly studied in a small subset of cell types that possess specific cellular thermogenesis machinery, including brown adipocytes, beige adipocytes, and muscle cells (Bal et al., 2012; Cannon and Nedergaard, 2004; Ikeda et al., 2017). Here, we identified a membrane lipid-mediated regulatory mechanism of intracellular temperature control in cells that are not specialized for thermogenesis. Moreover, the cell-autonomous increase in mitochondrial membrane potential during cold exposure was recently observed in cultured neurons differentiated from human-derived induced pluripotent stem cells (Ou et al., 2018). Although further investigations in other organisms are required, this study provides a framework for the control of intracellular temperature in living cells.

Limitations of the study

In this study, we identified a Δ9-desaturase-dependent mechanism underlying intracellular temperature control in *Drosophila* S2 cells. Components of our proposed system are present in most living cells. For example, SCD1, a predominant homolog of Δ9-desaturase in mammals, is ubiquitously expressed and is pivotal in unsaturated fatty acid biosynthesis (Ntambi and Miyazaki, 2004). Thus, although we evaluated the function of Δ9-desaturase only in *Drosophila* S2 cells, the Δ9-desaturase-dependent regulation of mitochondrial thermogenesis revealed in this study may contribute to cold adaptation in a wide range of cell types, including mammalian cells. However, mammalian cells are enriched in sterols and polyunsaturated fatty acids that affect the membrane properties, while S2 cells have only a small amount of these types of membrane lipids (Clark and Bloch, 1959; Matsuo et al., 2019). Thus, further studies in cells other than *Drosophila* cells involving specific interventions of Δ9-desaturase function together with careful evaluation of the global changes in the composition of membrane lipid molecules are required to demonstrate the generality of our findings in animal cells.

STAR★METHODS

Detailed methods are provided in the online version of this paper and include the following:

- KEY RESOURCES TABLE
- RESOURCE AVAILABILITY
  - Lead contact
  - Materials availability
  - Data and code availability

SUPPLEMENTAL INFORMATION

Supplemental information can be found online at https://doi.org/10.1016/j.celrep.2022.110487

ACKNOWLEDGMENTS

This work was supported by Grants-in-aid for Scientific research 15H05930 (to M.U.), 15K21744 (to M.U.), 20K21388 (to M.U.), 21H02477 (to M.U.), 15K07389 (to K.N.), 18K05433 (to K.N.), 21K05391 (to K.N.), 18H04695 (to R.S.), and 18J14529 (to A.M.) from the Japan Society for the Promotion of Science and Ministry of Education, Culture, Sports, Science and Technology. This work was performed in part under the Collaborative Research Program of Institute for Protein Research, Osaka University, CR-17-01, CR-18-01, and CR-19-01. The authors thank Shigeki Kiyonaka (Nagoya University) for valuable advice on the development of tsGFP1-LP variant, Masahiko Hatano (Kyoto University) for experimental supports in the development of tsGFP1-LP variant, Haruyasu Kohda and Keiko Furuta-Okamoto (Division of Electron Microscopic Study, Center for Anatomical Studies, Graduate School of Medicine, Kyoto University) for electron microscope analysis, and Junken Aoki (The University of Tokyo) for experimental supports in biochemical analysis.

AUTHOR CONTRIBUTIONS

M.U. conceived and designed the project. M.U. and K.N. supervised the research. A.M. performed most experiments with assistance from K.N., K.K., and Y. Hara. K.K. established *Desat1*-deficient cells. R.S. and Y.M. developed tsGFP1-LP variant. K.O. and Y. Harada supervised FPT analysis. A.M., K.N., and M.U. wrote the manuscript.

DECLARATION OF INTERESTS

The authors declare no competing interests.

Received: May 14, 2021
Revised: December 3, 2021
Accepted: February 14, 2022
Published: March 15, 2022

REFERENCES

Abdelwahid, E., Yokokura, T., Krieser, R.J., Balasundaram, S., Fowle, W.H., and White, K. (2007). Mitochondrial disruption in Drosophila apoptosis. Dev. Cell *12*, 793–806. https://doi.org/10.1016/j.devcel.2007.04.004.

Arselin, G., Vaillier, J., Salin, B., Schaeffer, J., Giraud, M.F., Dautant, A., Brethes, D., and Velours, J. (2004). The modulation in subunits e and g amounts of yeast ATP synthase modifies mitochondrial cristae morphology. J. Biol. Chem. *279*, 40392–40399. https://doi.org/10.1074/jbc.M404316200.

Bal, N.C., Maurya, S.K., Sopariwala, D.H., Sahoo, S.K., Gupta, S.C., Shaikh, S.A., Pant, M., Rowland, L.A., Bombardier, E., Goonasekera, S.A., et al. (2012). Sarcolipin is a newly identified regulator of muscle-based thermogenesis in mammals. Nat. Med. *18*, 1575–1579. https://doi.org/10.1038/nm.2897.

Bassett, A.R., Tibbit, C., Ponting, C.P., and Liu, J.L. (2014). Mutagenesis and homologous recombination in Drosophila cell lines using CRISPR/Cas9. Biol. Open *3*, 42–49. https://doi.org/10.1242/bio.20137120.

Bligh, E.G., and Dyer, W.J. (1959). A rapid method of total lipid extraction and purification. Can. J. Biochem. Physiol. *37*, 911–917. https://doi.org/10.1139/o59-099.

Boss, O., Samec, S., Kuhne, F., Bijlenga, P., Assimacopoulos-Jeannet, F., Seydoux, J., Giacobino, J.P., and Muzzin, P. (1998). Uncoupling protein-3 expression in rodent skeletal muscle is modulated by food intake but not by changes in environmental temperature. J. Biol. Chem. *273*, 5–8. https://doi.org/10.1074/jbc.273.1.5.

Brandner, K., Mick, D.U., Frazier, A.E., Taylor, R.D., Meisinger, C., and Rehling, P. (2005). Taz1, an outer mitochondrial membrane protein, affects stability and assembly of inner membrane protein complexes: implications for Barth Syndrome. Mol. Biol. Cell *16*, 5202–5214. https://doi.org/10.1091/mbc.e05-03-0256.

Cannon, B., and Nedergaard, J. (2004). Brown adipose tissue: function and physiological significance. Physiol. Rev. *84*, 277–359. https://doi.org/10.1152/physrev.00015.2003.

Chretien, D., Benit, P., Ha, H.H., Keipert, S., El-Khoury, R., Chang, Y.T., Jastroch, M., Jacobs, H.T., Rustin, P., and Rak, M. (2018). Mitochondria are physiologically maintained at close to 50 degrees C. PLoS Biol. *16*, e2003992. https://doi.org/10.1371/journal.pbio.2003992.

Civiletto, G., Varanita, T., Cerutti, R., Gorletta, T., Barbaro, S., Marchet, S., Lamperti, C., Viscomi, C., Scorrano, L., and Zeviani, M. (2015). Opa1 overexpression ameliorates the phenotype of two mitochondrial disease mouse models. Cell Metab. *21*, 845–854.

Clark, A.J., and Bloch, K. (1959). Absence OF sterol synthesis IN insects. J. Biol. Chem. *234*, 2578–2582.

Detmer, S.A., and Chan, D.C. (2007). Functions and dysfunctions of mitochondrial dynamics. Nat. Rev. Mol. Cell Biol. *8*, 870–879. https://doi.org/10.1038/nrm2275.

Duncan, A.L., Robinson, A.J., and Walker, J.E. (2016). Cardiolipin binds selectively but transiently to conserved lysine residues in the rotor of metazoan ATP synthases. Proc. Natl. Acad. Sci. U S A *113*, 8687–8692. https://doi.org/10.1073/pnas.1608396113.

Fedorenko, A., Lishko, P.V., and Kirichok, Y. (2012). Mechanism of fatty-acid-dependent UCP1 uncoupling in brown fat mitochondria. Cell *151*, 400–413. https://doi.org/10.1016/j.cell.2012.09.010.

Formosa, L.E., and Ryan, M.T. (2018). Mitochondrial OXPHOS complex assembly lines. Nat. Cell Biol. *20*, 511–513. https://doi.org/10.1038/s41556-018-0098-z.

Hardie, R.C. (2007). TRP channels and lipids: from Drosophila to mammalian physiology. J. Physiol. *578*, 9–24. https://doi.org/10.1113/jphysiol.2006.118372.

Hayashi, T., Fukuda, N., Uchiyama, S., and Inada, N. (2015). A cell-permeable fluorescent polymeric thermometer for intracellular temperature mapping in mammalian cell lines. PLoS One *10*, e0117677. https://doi.org/10.1371/journal.pone.0117677.

Hoch, F.L. (1992). Cardiolipins and biomembrane function. Biochim. Biophys. Acta *1113*, 71–133. https://doi.org/10.1016/0304-4157(92)90035-9.

Holthuis, J.C., and Menon, A.K. (2014). Lipid landscapes and pipelines in membrane homeostasis. Nature *510*, 48–57. https://doi.org/10.1038/nature13474.

Ikeda, K., Kang, Q., Yoneshiro, T., Camporez, J.P., Maki, H., Homma, M., Shinoda, K., Chen, Y., Lu, X., Maretich, P., et al. (2017). UCP1-independent signaling involving SERCA2b-mediated calcium cycling regulates beige fat thermogenesis and systemic glucose homeostasis. Nat. Med. *23*, 1454–1465. https://doi.org/10.1038/nm.4429.

Ikon, N., and Ryan, R.O. (2017). Cardiolipin and mitochondrial cristae organization. Biochim. Biophys. Acta Biomembr *1859*, 1156–1163. https://doi.org/10.1016/j.bbamem.2017.03.013.

Inomata, N., Toda, M., and Ono, T. (2016). Highly sensitive thermometer using a vacuum-packed Si resonator in a microfluidic chip for the thermal measurement of single cells. Lab Chip *16*, 3597–3603. https://doi.org/10.1039/c6lc00949b.

Joshi, A.S., Thompson, M.N., Fei, N., Huttemann, M., and Greenberg, M.L. (2012). Cardiolipin and mitochondrial phosphatidylethanolamine have overlapping functions in mitochondrial fusion in Saccharomyces cerevisiae. J. Biol. Chem. *287*, 17589–17597. https://doi.org/10.1074/jbc.M111.330167.

Kato, H., Sakaki, K., and Mihara, K. (2006). Ubiquitin-proteasome-dependent degradation of mammalian ER stearoyl-CoA desaturase. J. Cell Sci. *119*, 2342–2353. https://doi.org/10.1242/jcs.02951.

Kiyonaka, S., Kajimoto, T., Sakaguchi, R., Shinmi, D., Omatsu-Kanbe, M., Matsuura, H., Imamura, H., Yoshizaki, T., Hamachi, I., Morii, T., and Mori, Y. (2013). Genetically encoded fluorescent thermosensors visualize subcellular thermoregulation in living cells. Nat. Methods *10*, 1232–1238. https://doi.org/10.1038/nmeth.2690.

Kriszt, R., Arai, S., Itoh, H., Lee, M.H., Goralczyk, A.G., Ang, X.M., Cypess, A.M., White, A.P., Shamsi, F., Xue, R., et al. (2017). Optical visualisation of thermogenesis in stimulated single-cell brown adipocytes. Sci. Rep. *7*, 1383. https://doi.org/10.1038/s41598-017-00291-9.

Los, D.A., and Murata, N. (2004). Membrane fluidity and its roles in the perception of environmental signals. Biochim. Biophys. Acta *1666*, 142–157. https://doi.org/10.1016/j.bbamem.2004.08.002.

Matsuo, N., Nagao, K., Suito, T., Juni, N., Kato, U., Hara, Y., and Umeda, M. (2019). Different mechanisms for selective transport of fatty acids using a single class of lipoprotein in Drosophila. J. Lipid Res. *60*, 1199–1211. https://doi.org/10.1194/jlr.M090779.

Minkler, P.E., and Hoppel, C.L. (2010). Separation and characterization of cardiolipin molecular species by reverse-phase ion pair high-performance liquid chromatography-mass spectrometry. J. Lipid Res. *51*, 856–865. https://doi.org/10.1194/jlr.D002857.

Murakami, A., Nagao, K., Juni, N., Hara, Y., and Umeda, M. (2017). An N-terminal di-proline motif is essential for fatty acid-dependent degradation of Delta9-desaturase in Drosophila. J. Biol. Chem. *292*, 19976–19986. https://doi.org/10.1074/jbc.M117.801936.

Nagao, K., Murakami, A., and Umeda, M. (2019). Structure and function of delta9-fatty acid. Desaturase. Chem. Pharm. Bull. (Tokyo) *67*, 327–332. https://doi.org/10.1248/cpb.c18-01001.

Nakagawa, Y., Sakumoto, N., Kaneko, Y., and Harashima, S. (2002). Mga2p is a putative sensor for low temperature and oxygen to induce OLE1 transcription in Saccharomyces cerevisiae. Biochem. Biophys. Res. Commun. *291*, 707–713. https://doi.org/10.1006/bbrc.2002.6507.

Ntambi, J.M., and Miyazaki, M. (2004). Regulation of stearoyl-CoA desaturases and role in metabolism. Prog. Lipid Res. *43*, 91–104. https://doi.org/10.1016/s0163-7827(03)00039-0.

Okabe, K., Inada, N., Gota, C., Harada, Y., Funatsu, T., and Uchiyama, S. (2012). Intracellular temperature mapping with a fluorescent polymeric thermometer and fluorescence lifetime imaging microscopy. Nat. Commun. *3*, 705. https://doi.org/10.1038/ncomms1714.

Okabe, K., Sakaguchi, R., Shi, B., and Kiyonaka, S. (2018). Intracellular thermometry with fluorescent sensors for thermal biology. Pflugers Arch. *470*, 717–731. https://doi.org/10.1007/s00424-018-2113-4.

Oliveira, M.T., and Kaguni, L.S. (2011). Reduced stimulation of recombinant DNA polymerase gamma and mitochondrial DNA (mtDNA) helicase by variants of mitochondrial single-stranded DNA-binding protein (mtSSB) correlates with defects in mtDNA replication in animal cells. J. Biol. Chem. *286*, 40649–40658. https://doi.org/10.1074/jbc.M111.289983.

Ou, J., Ball, J.M., Luan, Y., Zhao, T., Miyagishima, K.J., Xu, Y., Zhou, H., Chen, J., Merriman, D.K., Xie, Z., et al. (2018). iPSCs from a hibernator provide a platform for studying cold adaptation and its potential medical applications. Cell *173*, 851–863.e816. https://doi.org/10.1016/j.cell.2018.03.010.

Paradies, G., Paradies, V., De Benedictis, V., Ruggiero, F.M., and Petrosillo, G. (2014). Functional role of cardiolipin in mitochondrial bioenergetics. Biochim. Biophys. Acta *1837*, 408–417. https://doi.org/10.1016/j.bbabio.2013.10.006.

Rabl, R., Soubannier, V., Scholz, R., Vogel, F., Mendl, N., Vasiljev-Neumeyer, A., Korner, C., Jagasia, R., Keil, T., Baumeister, W., et al. (2009). Formation of cristae and crista junctions in mitochondria depends on antagonism between Fcj1 and Su e/g. J. Cell Biol. *185*, 1047–1063. https://doi.org/10.1083/jcb.200811099.

Rahbani, J.F., Roesler, A., Hussain, M.F., Samborska, B., Dykstra, C.B., Tsai, L., Jedrychowski, M.P., Vergnes, L., Reue, K., Spiegelman, B.M., and Kazak, L. (2021). Creatine kinase B controls futile creatine cycling in thermogenic fat. Nature *590*, 480–485. https://doi.org/10.1038/s41586-021-03221-y.

Rouser, G., Siakotos, A.N., and Fleischer, S. (1966). Quantitative analysis of phospholipids by thin-layer chromatography and phosphorus analysis of spots. Lipids *1*, 85–86. https://doi.org/10.1007/bf02668129.

Schlame, M., Xu, Y., Erdjument-Bromage, H., Neubert, T.A., and Ren, M. (2020). Lipidome-wide (13)C flux analysis: a novel tool to estimate the turnover of lipids in organisms and cultures. J. Lipid Res. *61*, 95–104. https://doi.org/10.1194/jlr.D119000318.

Schneider, C.A., Rasband, W.S., and Eliceiri, K.W. (2012). NIH Image to ImageJ: 25 years of image analysis. Nat. Methods *9*, 671–675. https://doi.org/10.1038/nmeth.2089.

Schneider, I. (1972). Cell lines derived from late embryonic stages of Drosophila melanogaster. J. Embryol. Exp. Morphol. *27*, 353–365.

Sekiguchi, T., Sotoma, S., and Harada, Y. (2018). Fluorescent nanodiamonds as a robust temperature sensor inside a single cell. Biophys. Physicobiol. *15*, 229–234. https://doi.org/10.2142/biophysico.15.0_229.

Shiomi, A., Nagao, K., Yokota, N., Tsuchiya, M., Kato, U., Juni, N., Hara, Y., Mori, M.X., Mori, Y., Ui-Tei, K., et al. (2021). Extreme deformability of insect cell membranes is governed by phospholipid scrambling. Cell Rep. *35*, 109219. https://doi.org/10.1016/j.celrep.2021.109219.

Smiley, S.T., Reers, M., Mottola-Hartshorn, C., Lin, M., Chen, A., Smith, T.W., Steele, G.D., Jr., and Chen, L.B. (1991). Intracellular heterogeneity in mitochondrial membrane potentials revealed by a J-aggregate-forming lipophilic cation JC-1. Proc. Natl. Acad. Sci. U S A *88*, 3671–3675. https://doi.org/10.1073/pnas.88.9.3671.

Sun, Y., Rahbani, J.F., Jedrychowski, M.P., Riley, C.L., Vidoni, S., Bogoslavski, D., Hu, B., Dumesic, P.A., Zeng, X., Wang, A.B., et al. (2021). Mitochondrial TNAP controls thermogenesis by hydrolysis of phosphocreatine. Nature *593*, 580–585. https://doi.org/10.1038/s41586-021-03533-z.

Tatzer, V., Zellnig, G., Kohlwein, S.D., and Schneiter, R. (2002). Lipid-dependent subcellular relocalization of the acyl chain desaturase in yeast. Mol. Biol. Cell *13*, 4429–4442. https://doi.org/10.1091/mbc.e02-04-0196.

Tiku, P.E., Gracey, A.Y., Macartney, A.I., Beynon, R.J., and Cossins, A.R. (1996). Cold-induced expression of delta 9-desaturase in carp by transcriptional and posttranslational mechanisms. Science *271*, 815–818. https://doi.org/10.1126/science.271.5250.815.

Uto, Y., Ogata, T., Kiyotsuka, Y., Miyazawa, Y., Ueno, Y., Kurata, H., Deguchi, T., Yamada, M., Watanabe, N., Takagi, T., et al. (2009). Novel and potent inhibitors of stearoyl-CoA desaturase-1. Part II: identification of 4-ethylamino-3-(2-hydroxyethoxy)-N-[5-(3-trifluoromethylbenzyl)thiazol-2-yl]benza mide and its biological evaluation. Bioorg. Med. Chem. Lett. *19*, 4159–4166. https://doi.org/10.1016/j.bmcl.2009.05.123.

Vance, J.E. (1990). Phospholipid synthesis in a membrane fraction associated with mitochondria. J. Biol. Chem. *265*, 7248–7256.

VanEngelenburg, S.B., and Palmer, A.E. (2008). Fluorescent biosensors of protein function. Curr. Opin. Chem. Biol. *12*, 60–65. https://doi.org/10.1016/j.cbpa.2008.01.020.

Varanita, T., Soriano, M.E., Romanello, V., Zaglia, T., Quintana-Cabrera, R., Semenzato, M., Menabo, R., Costa, V., Civiletto, G., Pesce, P., et al. (2015). The OPA1-dependent mitochondrial cristae remodeling pathway controls atrophic, apoptotic, and ischemic tissue damage. Cell Metab. *21*, 834–844. https://doi.org/10.1016/j.cmet.2015.05.007.

Wieckowski, M.R., Giorgi, C., Lebiedzinska, M., Duszynski, J., and Pinton, P. (2009). Isolation of mitochondria-associated membranes and mitochondria from animal tissues and cells. Nat. Protoc. *4*, 1582–1590. https://doi.org/10.1038/nprot.2009.151.

Xu, Y., Malhotra, A., Ren, M., and Schlame, M. (2006). The enzymatic function of tafazzin. J. Biol. Chem. *281*, 39217–39224. https://doi.org/10.1074/jbc.M606100200.

STAR★METHODS

KEY RESOURCES TABLE

REAGENT or RESOURCE	SOURCE	IDENTIFIER
Antibodies		
rabbit polyclonal anti-DESAT1	(Murakami et al., 2017)	N/A
rabbit polyclonal anti-SESB	(Shiomi et al., 2021)	N/A
rabbit polyclonal anti-α Tubulin	MBL	PM054
mouse monoclonal anti-ATP5A	Abcam	#ab14748
rabbit polyclonal anti-CALNEXIN	Abcam	#ab13504
rabbit polyclonal anti-GFP	MBL	#598
rat monoclonal anti-HA	Roche	#12158167001
mouse monoclonal anti-HA	Santa Cruz Biotechnology	#sc-7392
MitoProfile Total OXPHOS Rodent Antibody Cocktail	Abcam	#ab110413
Chemicals		
DESAT1 inhibitor (SCD1 inhibitor 37c)	Daiichi Sankyo Co. Ltd (Uto et al., 2009)	DS18220913
Fluorescent polymeric thermometer	Funakoshi	#FDV-004
TransFectin Lipid Reagent	Bio-Rad	#1703350
Tetramethylrhodamine methyl ester (TMRM)	Thermo Fisher Scientific	#T668
Mitotracker Deep Red FM	Thermo Fisher Scientific	#M22426
JC-1	Dojindo Molecular Technologies	#MT09
Critical commercial assays		
CellTiter 96 AQueous One	PROMEGA	#G3582
ISOGEN II	NIPPON GENE	#317-07363
High-Capacity cDNA Reverse Transcription Kit	Thermo Fisher Scientific	#4368814
PowerUP SYBR Green Mater Kit	Thermo Fisher Scientific	#A25741
Super Signal West Pico	Thermo Fisher Scientific	#34080
MitoCheck Complex V Activity Assay Kit	Cayman Chemical	#701000
Pierce BCA protein Assay Kit	Thermo Fisher Scientific	#23227
Experimental models: cell lines		
D. melanogaster. S2 cells	Provided by Dr. Kumiko Ui-Tei	N/A
Experimental models: organisms/strains		
D. melanogaster. w[1118]; P{w[+mC]=UAS-mito-HA-GFP.AP}3,e[1]	Bloomington Drosophila Stock Center	#8443
Recombinant DNA		
cDNA *Opa1*	Drosophila Genomic Resource Center	GH13793
cDNA Bip-GFP-KDEL	Addgene	#69917
Plasmid: pAc5.1-V5-His-A	Thermo Fisher Scientific	#V411020
Plasmid: pAc-sgRNA-Cas9	Addgene	#49330
Software and algorithms		
imageJ	(Schneider et al., 2012)	https://imagej.nih.gov/ij
ZEN	Carl-Zeiss	https://www.zeiss.co.jp
JMP11	SAS Institute	https://www.jmp.com

RESOURCE AVAILABILITY

Lead contact

Further information and requests for resources and reagents should be directed to and will be fulfilled by the lead contact, Masato Umeda (umeda@sbchem.kyoto-u.ac.jp).

Materials availability

All expression plasmids and reagents will be shared upon request.

Data and code availability

All data generated and analyzed in this study are available from the corresponding author on reasonable request. The custom compute codes used to generate results in this study are available from the corresponding author on reasonable request. Any additional information required to reanalyze the data reported in this paper is available from the lead contact upon request.

EXPERIMENTAL MODEL AND SUBJECT DETAILS

Drosophila S2 cells (Schneider, 1972) were maintained in a culture medium (Schneider's Drosophila medium supplemented with 10% fetal bovine serum (FBS), 50 units/ml penicillin, and 50 μg/ml streptomycin) at 25°C. The bovine serum albumin (BSA)–fatty acid complex (1:9 molar ratio) was prepared by incubating fatty acid with a 0.9% NaCl solution containing BSA (111 mg/ml).

METHOD DETAILS

Construction of plasmids

The coding sequence of DESAT1 was isolated from a cDNA library of *Drosophila* strain Canton-S (Murakami et al., 2017). cDNA encoding *Drosophila* OPA1 (GH13793) was obtained from the Drosophila Genomics Resource Center and introduced into *Eco*RI and *Xho*I sites of the pAc5.1/V5-His A plasmid (Invitrogen). FLAG epitope tag (DYKDDDDDK) and HA epitope tag (YPYDVPDYA) were inserted into the C-terminal of the OPA1-coding sequence. The mitochondrial localization signal (the 29 N-terminal amino acid residues of human COX8) amplified from the genome DNA of a *Drosophila* strain harboring UAS-mito-HA-GFP (Bloomington Drosophila Stock Center, #8443) was inserted in *Eco*RI and *Xho*I sites of pAc5.1-EGFP plasmid to construct the pAc5.1-mito-EGFP. tsGFP1-LP was generated by introducing the mutations (TlpA-L137P) into two TlpA-derived domains of tsGFP1 (Kiyonaka et al., 2013) using site-directed mutagenesis. The pAc5.1-tsGFP1-LP was constructed by inserting the coding sequence of tsGFP1-LP into *Eco*RI and *Xho*I sites of pAc5.1/V5-His A plasmid. A mitochondrial localization sequence was fused with the coding sequence of tsGFP1-LP using a previously reported method (Kiyonaka et al., 2013). Recombinant tsGFP1 proteins were prepared as previously reported (Kiyonaka et al., 2013). Fluorescence excitation spectra were collected on Hitachi F2700 equipped with a temperature control unit using 0.5-cm quartz cuvette. The excitation spectra of protein (25 μM) in PBS were recorded from 300 nm to 500 nm. cDNA encoding Bip-GFP-KDEL (Addgene, #69917) was inserted in *Eco*RI and *Xho*I sites of pAc5.1/V5-His A plasmid to construct pAc5.1-Bip-GFP-KDEL.

S2 cells were transfected with an expression vector with pCoBlast plasmid using TransFectin Lipid Reagent (Bio-Rad), and stable transformants were selected using 20 μg/ml of blasticidin. When either pAc5.1-DESAT1-HA or pAc5.1-DESAT1-FLAG was transfected into *Desat1*-deficient cells, cells were cultured in the culture medium containing the BSA–fatty acid complex (50 μM C16:1 and 50 μM C18:1). At 24 h after the transfection, the medium was replaced by the culture medium without unsaturated fatty acids supplementation.

Disruption of the *Desat1* gene in S2 cells

pAc-sgRNA-Cas9-desat1-141 and pAc-sgRNA-Cas9-desat1-194 were constructed by ligating the synthesized oligonucleotides (for pAc-sgRNA-Cas9-desat1-141: 5'-TTCGCACCGACGGTGGTCTTGTCA-3' and 5'-AACTGACAAGACCACCGTCGGTGC-3', for pAc-sgRNA-Cas9-desat1-194: 5'-TTCGAGCGCCGCCTGAAGCTCGTC-3' and 5'-AACGACGAGCTTCAGGCGGCGCTC-3') into the BspQI sites of the pAc-sgRNA-Cas9 plasmid (Addgene, #49330) (Bassett et al., 2014). First, pAc-sgRNA-Cas9-desat1-141 was introduced into S2 cells using the TransFectin lipid reagent (Bio-Rad). After 2 weeks of puromycin selection (2.5 μg/ml) in the culture medium containing the BSA–fatty acid complex (100 μM C18:1), single-cell clones were isolated by limiting dilution. Next, the isolated clone was transfected with pAc-sgRNA-Cas9-desat1-194 and incubated in the culture medium containing the BSA–fatty acid complex (100 μM C18:1) and 2.5 μg/ml puromycin for 2 weeks. Single-cell clones were isolated by limiting dilution in the culture medium containing the BSA–fatty acid complex (100 μM C18:1). Established DESAT1-deficient cells were maintained in the culture medium containing the BSA–fatty acid complex (50 μM C16:1 and 50 μM C18:1).

Measurement of Δ9-desaturase activity

Cells were incubated with a BSA–margaric acid (C17:0) complex (20 μM C17:0) in Schneider's Drosophila medium supplemented with 50 units/ml penicillin and 50 μg/ml streptomycin for 6 h. Conversion of C17:0 to heptadecenoic acid (C17:1) was evaluated using gas chromatography as described in the following. The Δ9-desaturase activity was defined as the ratio of the amount of C17:1 to the total amount of C17 fatty acid species.

Evaluation of cell growth

Cells in a 48-well plate were incubated for 72 h in 300 μL of the culture medium. To evaluate the number of living cells, 40 μL of CellTiter AQueous One (PROMEGA) was added to each well. After 1 h of incubation at 25°C, the absorbance at 490 nm was measured using infinite F200 PRO (Tecan).

Temperature imaging with a fluorescent polymeric thermometer

Cells were cultured in a 35-mm glass-bottomed dish (glass 14 φ, Iwaki) in the culture medium at 25°C. Cells were incubated in 150 μl of 5% glucose solution containing 0.01% cell-permeable fluorescent polymeric thermometer (FPT) (Funakoshi) (Hayashi et al., 2015) at 25°C for 10 min and washed twice with phosphate-buffered saline (PBS). A TCS-SP8 confocal laser-scanning microscope (Leica) equipped with a 405-nm laser (PDL 800-B, PicoQuant, Berlin, Germany) and a TCSPC module SPC-830 (Becker & Hickl, Berlin, Germany) were used for fluorescence lifetime imaging microscopy (FLIM) analysis and confocal fluorescence imaging. For FLIM analysis, the pulse repetition rate of the 470-nm laser was set at 20 MHz. The fluorescence was captured with an HCX PL APO Ibd.BL 63 × 1.4 N.A. oil objective (Leica) with zoom factor of 6 in 128 × 128-pixel format and pinhole size of 2 units at 100 Hz scanning speed (scanning duration set to 30 or 60 s) through a 500–700 nm bandpass filter. To simultaneously measure intracellular temperature and mitochondrial membrane potential, cells treated with FPT were stained with 10 nM tetramethylrhodamine methyl ester (TMRM) (Thermo Fisher Scientific) in PBS containing 0.01% BSA for 20 min at 25°C and washed twice with PBS. FPT fluorescence lifetime imaging was performed as described above, except that emitted light was collected using a 500–540 nm bandpass filter. A 552-nm optically pumped semiconductor laser (OPSL) was used to excite TMRM and resulting TMRM fluorescence was collected using a 560–700 nm bandpass filter. During FLIM analysis, cells were maintained in PBS containing 0.01% BSA, and the temperature of the medium was controlled with a stage insert (Carl Zeiss) and monitored using a thermocouple (MC-1000, Tokai-Hit). The fluorescence lifetime images were obtained using SymPhoTime's FAST FLIM software (PicoQuant, RRID:SCR_016263). The obtained fluorescence decay curve was fitted with a double-exponential function using SymPhoTime software (PicoQuant) using the following equation (Equation 1):

$$I(t) = A_1 \exp\left(\frac{-t}{\tau_1}\right) + A_2 \exp\left(\frac{-t}{\tau_2}\right) \quad \text{(Equation 1)}$$

Then the fluorescence lifetime (τ_f) (ns) was calculated using the following equation (Equation 2):

$$\tau_f = \frac{(A_1\tau_1^2 + A_2\tau_2^2)}{(A_1\tau_1 + A_2\tau_2)} \quad \text{(Equation 2)}$$

The fluorescence lifetime for each pixel was calculated using Equation 2 and averaged within the whole pixels of a single cell. The average FPT fluorescence lifetime in each cell is plotted in Figures 1, 3, S1 and S3. In the experiments using oligomycin or carbonyl cyanide *p*-trifluoromethoxyphenylhydrazone (FCCP), the intracellular temperature was measured within 30 min after the treatment with these reagents.

The fluorescence intensity of TMRM was quantified using ImageJ software. The integrated fluorescence density in each cell was plotted in Figure S1D.

Temperature imaging with a genetically encoded protein-based thermometer

Cells transfected with pAc5.1-tsGFP1-LP or pAc5.1-tsGFP1-LP-mito were plated on a 35-mm glass-bottomed dish (glass 14 φ, Iwaki) in the culture medium. Fluorescence images were acquired with a confocal laser-scanning microscope (LSM 800; Carl Zeiss) with a 63× objective lens using a diode laser (405-nm line), an argon laser (488-nm line), and bandpass filter (505–525 nm). During confocal microscope observation, cells were maintained in PBS containing 0.01% BSA, and the temperature of the medium was controlled using a stage insert (PECON Heating Insert P 2000) and monitored using a thermocouple (TA-29, CL-100; Physio-Tech). Ratiometric images (ex405/ex488) were obtained using ZEN software (Carl Zeiss) from two images (excitation at 405 nm, emission at 505–525 nm, and excitation at 488 nm, emission at 505–525 nm) and shown in rainbow color. The ratio of fluorescent intensity was quantified using ImageJ software, and the average value in each cell was calculated. The value of the Δ ratio was calculated by subtracting the average value of ex405/ex488 ratio for the genetically encoded protein-based thermometer (tsGFP1-LP) in control cells from the value of ex405/ex488 ratio of the tsGFP1-LP in each cell and is plotted in Figures 1, 2, and 4. In the experiments using rotenone, the intracellular temperature was measured within 30 min after the rotenone treatment. Mitotracker Deep Red FM (Thermo Fisher Scientific) was used for staining the mitochondria in S2 cells.

Measurement of mitochondrial DNA content

The mitochondrial DNA content was analyzed following a previously described protocol (Oliveira and Kaguni, 2011). In brief, total DNA was extracted from S2 cells using phenol/chloroform/isoamyl alcohol (25:24:1) (NIPPON GENE) and washed with 70% ethanol. The amounts of DNA encoding mitochondrial 16S (as mitochondrial DNA) and *Rpl32* (as nuclear DNA) were analyzed using the StepOnePlus real-time polymerase chain reaction (PCR) system (Thermo Fisher Scientific) with PowerUP SYBR Green Master Mix (Thermo Fisher Scientific) and the specific primers (for mitochondrial 16S: 5'-AAAAAGATTGCGACCTCGAT-3' and 5'-AAACC AACCTGGCTTACACC-3', for *Rpl32*: 5'-GGCCCAAGATCGTGAAGAA-3' and 5'-TGTGCACCAGGAACTTCTTGAA-3'). Relative amounts of mitochondrial DNA to nuclear DNA were defined as the mitochondrial DNA content.

Quantification of *Opa1* gene expression by RT-qPCR

The total RNA was extracted using ISOGEN II (NIPPON GENE). The cDNA was prepared using High-Capacity cDNA Reverse Transcription Kit (Thermo Fisher Scientific). The expression level of *Opa1* mRNA was quantified using Light Cycler 96 system (Roche) with PowerUP SYBR Green Master Mix (Thermo Fisher Scientific) and specific primers (for *Opa1*, 5′-TCCCCAGATTGCGCGAG-3′ and 5′-CAGCGGGCAGATAGATGCTT-3′; for *Rp49*, 5′-CCAAGCACTTCATCCGCCACC-3′ and 5′-GCGGGTGCGCTTGTTCGATCC-3′) and quantified using the $2^{-\Delta\Delta Ct}$ method.

Measurement of mitochondrial membrane potential with a JC-1 probe

Mitochondrial membrane potential in S2 cells was evaluated using JC-1 (Dojindo Molecular Technologies), a lipophilic membrane-permeant cation that selectively enters mitochondria and exists in a monomeric form (green fluorescence) or in an aggregated form (red fluorescence) upon mitochondrial hyperpolarization (Smiley et al., 1991). Cells were incubated with JC-1 (5 μM) for 30 min at culture temperature (25 or 15°C) and were washed twice with PBS. During microscope observation, cells were maintained in PBS containing 0.01% BSA. For the experiments shown in Figures 3, S3 and S6 fluorescence images were obtained with a confocal laser-scanning microscope (LSM 800; Carl Zeiss) with a 63× objective lens using a paired argon laser (488-nm line) and bandpass filter (400–545 nm) and a paired HeNe laser (561-nm line) and long-pass filter (545 nm). The temperature of the medium was controlled using a stage insert (PECON Heating Insert P 2000) and monitored using a thermocouple (TA-29, CL-100; Physio-Tech). For the experiments shown in Figure 6, fluorescence images were acquired with a microscope (Axio-observer Z1) with a 40× objective lens. JC-1 fluorescence was excited at 488 and 561 nm. The emission was obtained between 515/545 and 575/625 nm. The temperature of the medium was controlled in a perfusion chamber with a controller (SC-20, CL-100; Physio-Tech) and monitored using a thermocouple (TA-29, CL-100; Physio-Tech). Ratiometric images (ex561/ex488) were analyzed with ZEN software (Zeiss) and quantified with ImageJ. The average value in each cell was calculated.

Mitochondrial membrane potential recovery assay

We conducted a time course analysis of the changes in the mitochondrial membrane potential to evaluate the dynamics of proton gradient formation in the mitochondria. The cells were incubated with JC-1 (5 μM) for 30 min at culture temperature (25°C or 15°C) and then washed with PBS, followed by incubation with rotenone (5 μM) for 30 min to depolarize the mitochondria. After washing with PBS twice, mitochondrial membrane potential was recorded. During microscopic observation, the cells were maintained in Schneider's Drosophila medium without FBS supplementation at 25°C.

Measurement of the oxygen consumption rate

The oxygen consumption rate (OCR) in S2 cells was measured using the Seahorse XFe Extracellular Flux Analyzer (Agilent) in a 96-well plate. Briefly, cells were plated into poly-L-lysine-coated seahorse 96-well plates and preincubated in the culture medium for 16 h in the presence or absence of DESAT1 inhibitor (1 μM). Before the measurement, the medium was exchanged with XF assay medium. The cells were subjected to mitochondrial stress tests by adding oligomycin (3 μM) followed by FCCP (1 μM), with a mixture of rotenone (0.5 μM) and antimycin A (0.5 μM). Oligomycin is an inhibitor of mitochondrial F_1F_o-ATPase that suppresses the ATP synthesis-dependent OCR. FCCP is a chemical uncoupler that maximizes the electron transfer activity of mitochondrial complex I–IV independent of ATP synthesis. Rotenone and antimycin are inhibitors of mitochondrial complexes I and III, respectively.

Transmission electron microscopy

The S2 cells were fixed in 10 mM phosphate butter (pH 7.4) containing 2.5% glutaraldehyde and 2.5% formaldehyde for 16 h, washed with 10 mM phosphate buffer (pH 7.4), postfixed with 1% osmium tetraoxide in 10 mM phosphate buffer (pH 7.4), dehydrated through an ethanol series, embedded in epoxy-resin Luveak (Nacalai Tesque), and polymerized at 60°C for 3 days. The specimen were cut into ultrathin sections (70 nm) on an ultramicrotome (EM UC6; Leica). The ultrathin sections were mounted on mesh grids, stained with uranyl acetate and lead citrate, and observed with an H-7650 electron microscope (Hitachi).

Blue native polyacrylamide gel electrophoresis

Oligomer formation of F_1F_o-ATPase was evaluated using polyacrylamide gel electrophoresis (PAGE) using a NativePAGE Novex Bis-Tris Gel System (Life Technologies). The cells were washed with ice-cold PBS and suspended in blue native (BN) sampling buffer (50 mM Bis-Tris-HCl (pH 7.2), 50 mM NaCl, 10% Glycerol, 0.001% Ponceau S, 1% digitonin, and 1% protease inhibitors (Nacalai Tesque)) on ice. After pipetting 20 times, cell lysates were centrifuged at 20,000 × g for 30 min at 4°C. Then, 40 μl of the supernatant was mixed with 2 μl of BN sampling buffer containing 5% Coomassie blue G-250. The samples were loaded onto NativePAGE Novex 4–16% (w/v) Bis-Tris gels (Life Technologies) and subjected to electrophoresis at 150 V for 30 min at 4°C. The CBB G-250 concentration in running buffer was changed from 0.02% to 0.002%, and the samples were further electrophoresed at 150 V for 120 min.

SDS-PAGE

Cells were washed with PBS and lysed in lysis buffer (10 mM Tris-HCl (pH 7.4), 1% Triton X-100, 0.1% sodium dodecyl sulfate (SDS), 1% sodium deoxycholate) containing 1% protease inhibitors (Nacalai Tesque). The lysates were centrifuged at 14,000 × g for 10 min

at 4°C. Then 40 μl of supernatant was mixed with 10 μl of SDS sampling buffer 1 (50 mM Tris-HCl (pH 8.0), 50% sucrose, 1% SDS, 5 mM ethylenediamine tetraacetic acid (EDTA), 0.4% bromophenol blue) and incubated for 10 min at 50°C, followed by mixing with 50 μl of SDS sampling buffer 2 (10 mM Tris-HCl (pH 8.0), 10% sucrose, 0.2% SDS, 1 mM EDTA, 0.08% bromophenol blue, 60% urea). The samples were electrophoresed on 10% or 5–20% (w/v) SDS-polyacrylamide gel.

Immunoblotting

Samples electrophoresed on SDS-polyacrylamide gels or NativePAGE Novex 4–16% (w/v) Bis-Tris gels were blotted on polyvinylidene fluoride (PVDF) membranes (Wako) using Trans-Blot SD Semi-Dry Electrophoretic Transfer Cells (Bio-Rad). Immunoblotting analysis was performed using rabbit anti-DESAT1 antibody (1:1,000), rabbit anti-SESB antibody (1:4,000), mouse anti-ATP5A antibody (1:4,000, abcam, #ab14748), rat anti-HA antibody (1:4,000, Roche, #12158167001), rabbit anti-GFP antibody (1:500, MBL, #598), rabbit anti-CALNEXIN antibody (1:500, abcam, #ab13504), MitoProfile Total OXPHOS Rodent Antibody Cocktail (1:1,000, abcam, #ab110413), and rabbit anti-α Tubulin antibody (1:1,000, MBL, #PM054) as the loading control. Bound antibodies were detected with horseradish peroxidase-conjugated anti-rabbit immunoglobulin (Ig) G antibody, anti-mouse IgG antibody, and anti-rat IgG using Super Signal West Pico (Thermo Scientific) and Ez-Capture MG (Atto). Rabbit polyclonal antibodies against DESAT1and SESB were generated against an 18-residue contiguous segment (DQPKEEIEDAVITHKKSE) of DESAT1 (Murakami et al., 2017) and a 17-residue contiguous segment (MGKDFDAVGFVKDFAAC) of SESB (Shiomi et al., 2021), respectively. Band intensities were determined using ImageJ software. The levels of F_1F_o-ATPase oligomer are shown relative to the amount of F_1F_o-ATPase monomer. The levels of ATP5A proteins are shown relative to the amount of ATP5A protein in control cells.

Measurement of F_1F_o-ATPase activity

F_1F_o-ATPase activity was detected using the MitoCheck Complex V Activity Assay Kit (Cayman Chemical) according to the manufacturer's instructions. Briefly, the cells were washed with PBS and homogenized in SET buffer (10 mM Tris-HCl (pH 7.4), 250 mM sucrose, 1 mM EGTA) using a Dounce homogenizer. The homogenate was centrifuged at 600 × g for 10 min twice to remove nuclei and debris. The collected supernatant was centrifuged for 30 min at 11,000 × g for obtaining crude mitochondria as precipitate. The crude mitochondria fraction was suspended in the assay buffer included in the MitoCheck Complex V Activity Assay Kit. The protein concentration of the crude mitochondria fraction was determined using the Pierce BCA Protein Assay Kit (Thermo Fisher Scientific). Solution A (0.1 mg protein/ml crude mitochondria fraction and 4 μM rotenone in the assay buffer), solution B (DMSO or 5 μM oligomycin in the assay buffer), and solution C (1.1 mM NADH and 2 mM ATP in the assay enzyme mix included in the MitoCheck Complex V Activity Assay Kit) were prepared. Then 30 μl of solution A was added to each well of the half-volume 96-well clear plate, followed by the addition of 20 μl of solution B and 50 μl of solution C. Using Spark 10M (TECAN), the absorbance at 340 nm (A_{340}) was measured at 30-s intervals for 30 min at 25°C. The F_1F_o-ATPase activity was defined as the rate of the increase of A_{340} (A_{340}/min).

Immunostaining

The S2 cells were fixed in PBS containing 4% formaldehyde for 30 min at 25°C, washed with PBS, permeabilized using 0.1% Triton X-100 in PBS for 5 min at 25°C, and finally washed with PBS. Immunostaining analysis was performed using mouse anti-HA antibody (1:100, Santa Cruz Biotechnology, #sc-7392). Bound antibody was detected with Alexa Fluor 633-conjugated anti-mouse IgG antibody (Thermo Fisher Scientific).

Organelle fractionation

Organelle fractionation of the S2 cells was performed following a previously described protocol (Wieckowski et al., 2009). Cells harvested from a 100-mm culture dish were washed with PBS and homogenized in buffer A (30 mM Tris-HCl (pH 7.4), 225 mM mannitol, 75 mM sucrose, 0.1 mM EGTA, 1% protease inhibitor (nacalai tesque)) using a Dounce homogenizer. Then the homogenate was centrifuged at 600 × g for 10 min twice in order to remove nuclei and debris. The collected supernatant was centrifuged for 10 min at 9,000 × g to obtain the crude mitochondria fraction. The supernatant was further centrifuged at 20,000 × g for 1 h. Then the supernatant was collected as the ER fraction, while the pellet was suspended in buffer A for obtaining the intermediate fraction. For further purification, the crude mitochondria fraction was suspended in buffer B (30 mM Tris-HCl (pH 7.4), 225 mM mannitol, 75 mM sucrose) and was centrifuged for 10 min at 10,000 × g. The pellet was suspended in buffer A. Immunoblotting was performed using rabbit anti-SESB antibody (1:4,000), mouse anti-ATP5A antibody (1:4,000, abcam, #ab14748), rabbit anti-CALNEXIN antibody (1:500, abcam, #ab13504), rabbit anti-GFP antibody (1:1,000, MBL, #598), and rabbit anti-DESAT1 antibody (1:1,000).

Lipid extraction and gas chromatography analysis of phospholipids

Total lipids were extracted using the Bligh and Dyer procedures (Bligh and Dyer, 1959). Phospholipids were separated using thin-layer chromatography (TLC) using hexane/diethyl ether/acetic acid (60:40:1, v/v/v) and incubated with methanolic HCl at 100°C for 3 h. Fatty acid methyl esters were extracted and analyzed using gas chromatography (GC) with a Shimadzu GC-14A with a flame ionization detector and an Omegawax Capillary GC column (Supelco). The temperatures of the injector and the flame ionization detector were held at 200°C and 280°C, respectively. The column temperature was programmed as follows: hold at 180°C for 5 min,

ramp to 220°C at 3°C/min, hold for 7 min, ramp to 240°C at 3°C/min, and hold for 10 min. The peak areas of methyl esters of C14:0, C14:1, C16:0, C16:1, C18:0, C18:1, C20:0, C20:4, and C20:5 were determined. The amount of phospholipids was determined using inorganic phosphate quantification (Rouser et al., 1966).

Liquid chromatography–mass spectroscopy analysis of phospholipids

The analysis of phospholipids was performed on a Shimadzu LC-30AD high-performance liquid chromatography (HPLC) system coupled to a triple-quadrupole LCMS-8040 mass spectrometer equipped with an electrospray source (Matsuo et al., 2019). Separation was performed on a Kinetex C8 column (2.6 μm; 2.1 × 150 mm; Phenomenex) with a binary mobile phase having the following composition: 10 mM ammonium formate in water (mobile phase A) and 10 mM ammonium formate in 2-propanol/acetonitrile/water (45:45:10; v/v/v) (mobile phase B). The pump controlling the gradient of mobile phase B was programmed as follows. Phosphatidylethanolamine (PE) and phosphatidylcholine (PC) analysis: an initial isocratic flow at 20% B for 1 min, a linear increase to 40% B for 1 min, an increase to 92.5% B using a curved gradient for 23 min, a linear increase to 100% B for 1 min, and a hold at 100% B for 4 min. Cardiolipin (CL) analysis: an initial isocratic flow at 20% B for 1 min, a linear increase to 80% B for 2 min, an increase to 100% B using a curved gradient for 30 min, and a hold at 100% B for 5 min. The total flow rate was 0.3 ml/min, the column temperature was 45°C, and the sample temperature was 4°C. The spectrometer parameters were as follows: nebulizer gas flow, 2 L/min; drying gas flow, 15 L/min, interface voltage, 4.5 kV; DL temperature, 250°C; and heat-block temperature, 400°C. The multiple reaction monitoring transition was $[M + H]^+ \rightarrow [M + H - 141.0]^+$ for PE and $[M + H]^+ \rightarrow [184.1]^+$ for PC. For CL analysis, deprotonated cardiolipin ions were detected. The fatty-acid composition of PE, PC, and CL was determined using product scan analysis of $[M - H]^-$, $[M + HCOO]^-$, and $[M - H]^-$ as precursor ions, respectively.

QUANTIFICATION AND STATISTICAL ANALYSIS

The statistical significance of differences between the mean values was analyzed using a nonpaired *t* test (two-sided). Multiple comparisons were performed using Tukey's test following analysis of variance (ANOVA). The relation between fluorescence lifetime of FPT and integrated fluorescence density of TMRM was evaluated by Pearson's correlation coefficient test. A p value of <0.05 was considered statistically significant. The measurements were taken from at least three independent samples.

Cell Reports, Volume *38*

Supplemental information

Cell-autonomous control of intracellular temperature by unsaturation of phospholipid acyl chains

Akira Murakami, Kohjiro Nagao, Reiko Sakaguchi, Keisuke Kida, Yuji Hara, Yasuo Mori, Kohki Okabe, Yoshie Harada, and Masato Umeda

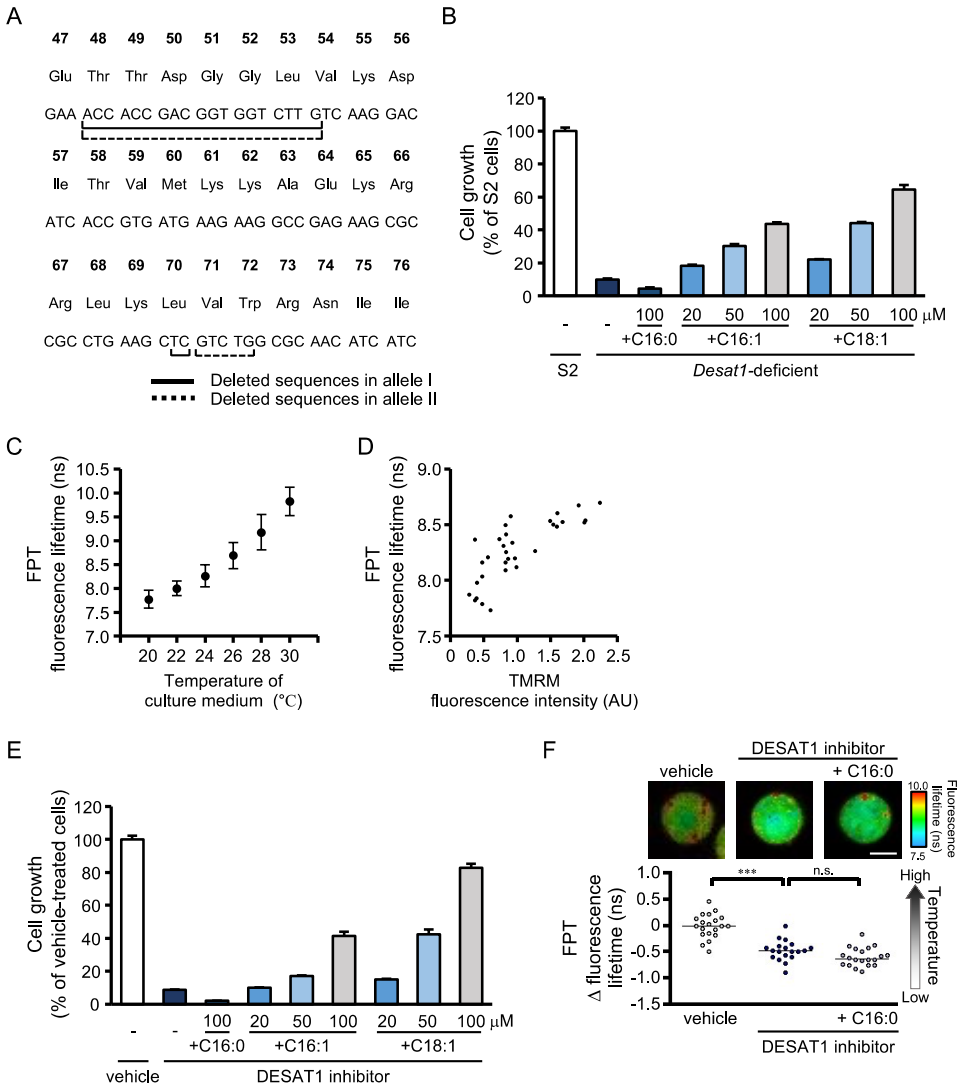

Figure S1. Characterization of DESAT1-suppressed cells and intracellular temperature imaging using FPT. Related to **Figure 1.**

(A) Mutations in *Desat1*-deficient cells. The solid lines and dotted lines represent the deleted sequence in allele I and allele II of *Desat1*-deficinet cells, respectively. The deletions in the *Desat1* gene caused frame shifts in each allele. (B) Effect of *Desat1* deletion on cell growth. *Desat1*-deficient cells were incubated in the culture medium supplemented with indicated concentrations of unsaturated fatty acids. As a control, S2 cells were incubated in the culture medium without unsaturated fatty acid supplementation. (C) Culture medium temperature-dependent changes in the FPT fluorescence lifetime in S2 cells. Mean ± SD (n = 17 at each temperature). (D) Relationship between the fluorescence lifetime of FPT and fluorescence intensity of TMRM in single cells at 25°C. Pearson's correlation coefficient test indicates the correlation (r = 0.786). (E) Effect of DESAT1 inhibitor (1 μM) on cell growth. S2 cells were incubated in the DESAT1 inhibitor-containing culture medium supplemented with indicated concentrations of unsaturated fatty acids. (F) Effect of C16:0 supplementation on the DESAT1 inhibitor-induced decrease in intracellular temperature of S2 cells. The medians are shown as lines. Scale bar indicates 5 μm. The average value in each cell was plotted (D, F). ***P < 0.001. n.s., not significant.

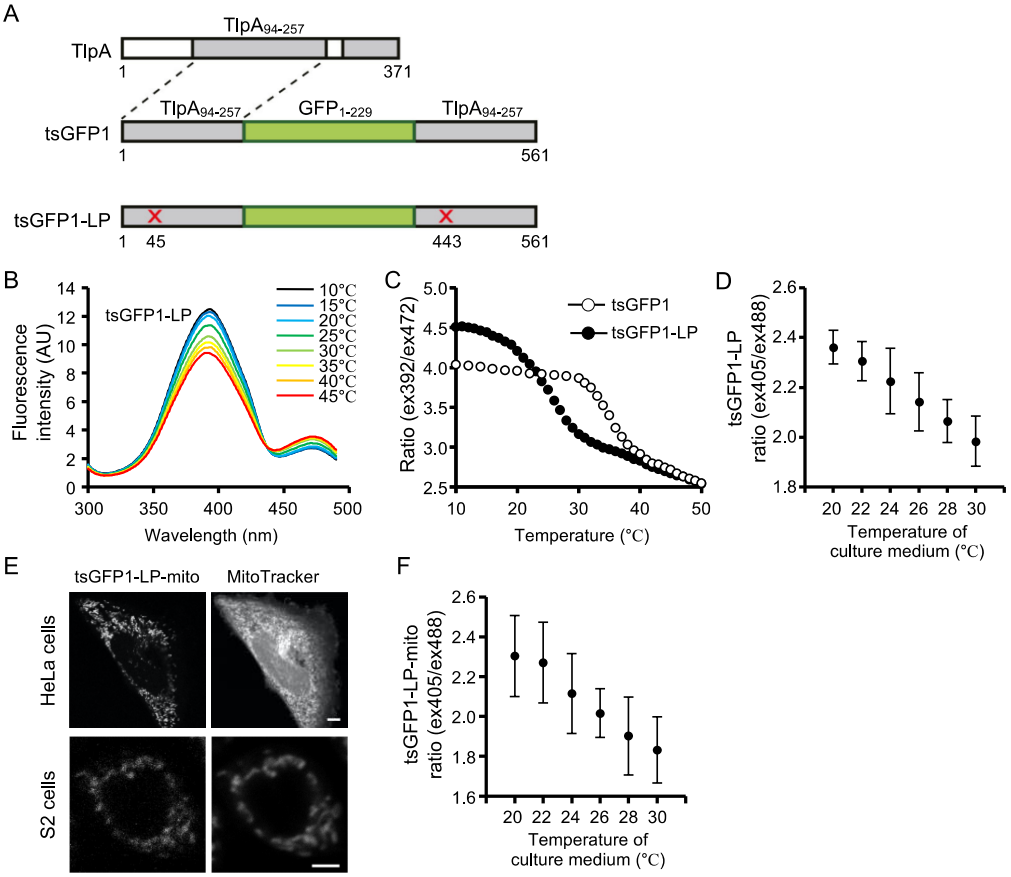

Figure S2. Intracellular temperature imaging using tsGFP1-LPs. Related to **Figures 1 and 2.**
(A) Schematic diagram of the tsGFP thermosensors. Coiled-coil regions of TlpA are shown in gray. GFP (green) is inserted in frame in between the tandemly repeated coiled-coil regions of TlpA. The leucine-to-proline mutations are indicated by red crosses. (B) Fluorescence excitation spectra of tsGFP1-LP at various temperatures. Emission is monitored at 510 nm. (C) Temperature-dependent changes in the ex397/ex472 ratio of tsGFP1 and tsGFP1-LP. (D) Culture medium temperature-dependent changes in the ex405/ex488 ratio of tsGFP1-LP in S2 cells. Mean ± SD ($n \geq 21$ at each temperature). (E) Confocal images of HeLa cells (upper) and S2 cells (lower) expressing tsGFP1-LP-mito. tsGFP1-LP-mito was successfully colocalized with a mitochondrial marker, MitoTracker Deep Red. (F) Culture medium temperature-dependent changes in the ex405/ex488 ratio of tsGFP1-LP-mito in S2 cells. Mean ± SD ($n \geq 12$). Scale bar indicates 5 μm.

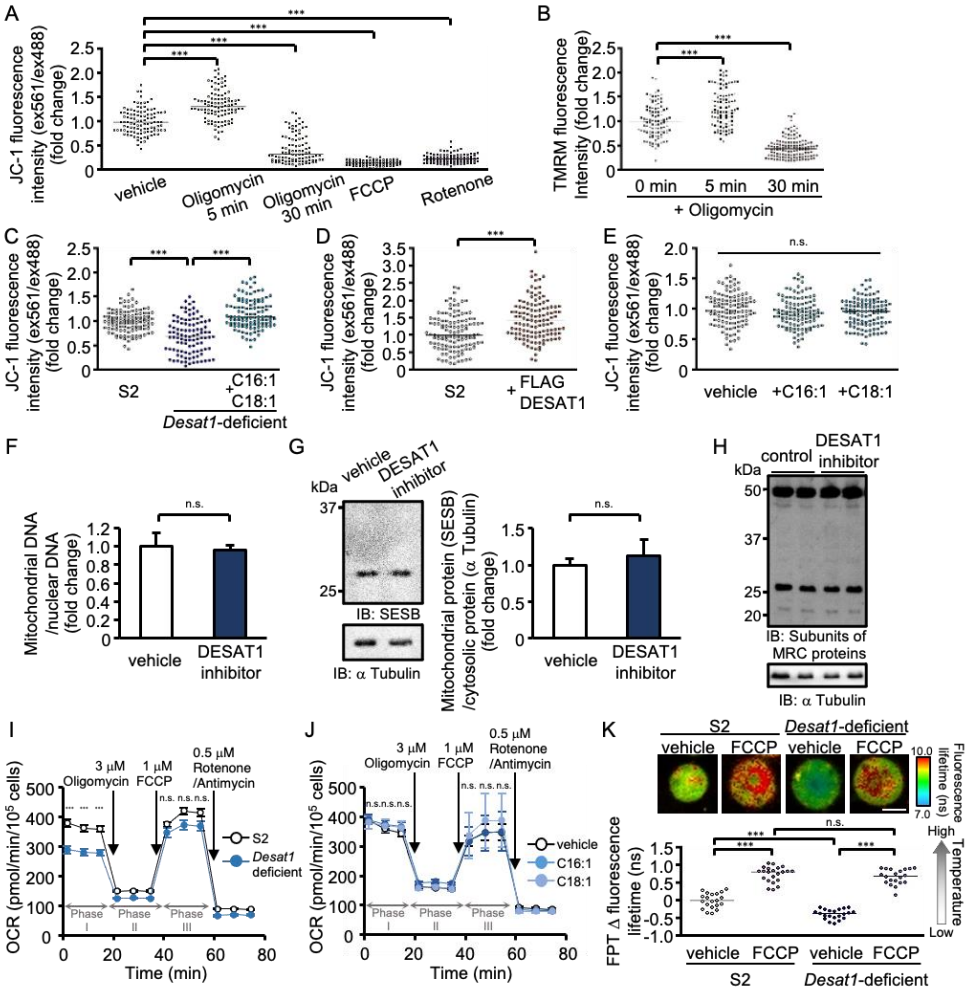

Figure S3. Regulation of mitochondrial membrane potential and ATP-synthesis dependent mitochondrial respiration by DESAT1. Related to **Figure 3.**

(A) Effect of treatment with oligomycin (3 μM) or the metabolic inhibitors on mitochondrial membrane potential evaluated by JC-1. S2 cells were treated with FCCP (5 μM) or rotenone (5 μM) for 15 min or 30 min, respectively. (B) Effect of treatment with oligomycin (3 μM) on mitochondrial membrane potential evaluated by TMRM. Effect of *Desat1* deletion (C) or DESAT1 overexpression (D) on mitochondrial membrane potential evaluated by JC-1. (E) Effect of treatment with unsaturated fatty acids (100 μM) for 16 h on mitochondrial membrane potential evaluated by JC-1. (F) Effect of treatment with the DESAT1 inhibitor (1 μM) for 16 h on the amount of mitochondrial DNA. Mean ± SD (n = 3). (G) Effect of treatment with the DESAT1 inhibitor (1 μM) for 16 h on the amount of SESB, a mitochondrial protein. The amount of SESB was normalized with that of α Tubulin. The levels of SESB proteins are shown relative to the amount of SESB protein in vehicle-treated cells. Mean ± SD (n = 3). (H) Effect of treatment with the DESAT1 inhibitor (1 μM) for 16 h on the amounts of mitochondrial respiratory chain (MRC) complex proteins. The subunits of the MRC complex proteins were detected using MitoProfile Total OXPHOS Rodent Antibody Cocktail. Effect of *Desat1* deletion (I) or treatment with unsaturated fatty acids (100 μM) for 16 h (J) on the oxygen consumption rate (OCR). Mean ± SE (n = 3, 6, respectively.). (K) Effect of treatment with FCCP (5 μM) for 15 min on FPT fluorescence lifetime in *Desat1*-deficient cells. Scale bar indicates 5 μm. The average value in each cell was calculated (A-E, K). The medians are shown as lines (A-E, K). ***P < 0.001. n.s., not significant.

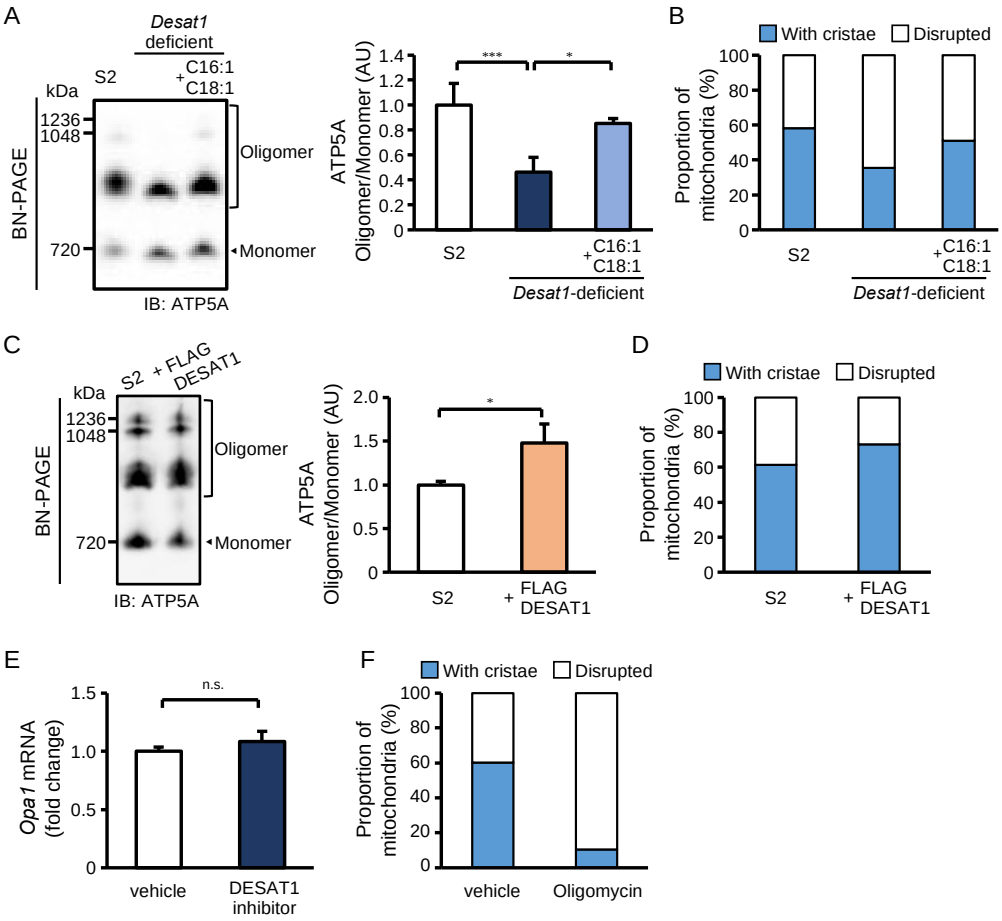

Figure S4. DESAT1-dependent regulation of F_1F_o-ATPase complex via cristae remodeling. Related to **Figure 4.**

(A) Effect of *Desat1* deletion on the oligomerization of F_1F_o-ATPase. The levels of F_1F_o-ATPase oligomer are shown relative to the amount of F_1F_o-ATPase monomer. (B) Effect of *Desat1* deletion on the mitochondrial structure. The proportions of mitochondria classified as in Figure 4C in S2 cells (n = 158) and *Desat1*-deficient cells cultured in a normal medium without or with unsaturated fatty acids (C16:1 and C18:1) supplementation (n = 180, 149). (C) Effect of DESAT1 overexpression on the oligomerization of F_1F_o-ATPase. The levels of F_1F_o-ATPase oligomer are shown relative to the amount of F_1F_o-ATPase monomer. (D) Effect of DESAT1 overexpression on the mitochondrial structure. The proportions of mitochondria classified as in Figure 4C in S2 cells (n = 129) and FLAG-DESAT1-overexpressing S2 cells (n = 150). (E) Effect of DESAT1 inhibitor (1 μM) for 16 h on the expression level of *Opa1* mRNA. Mean ± SD (n = 3). (F) Effect of treatment with oligomycin (3 μM) for 30 min on the mitochondrial structure. The proportions of mitochondria classified as in Figure 4C in vehicle-treated S2 cells (n = 101) and oligomycin-treated S2 cells (n = 104). *P < 0.05, ***P < 0.001. n.s., not significant.

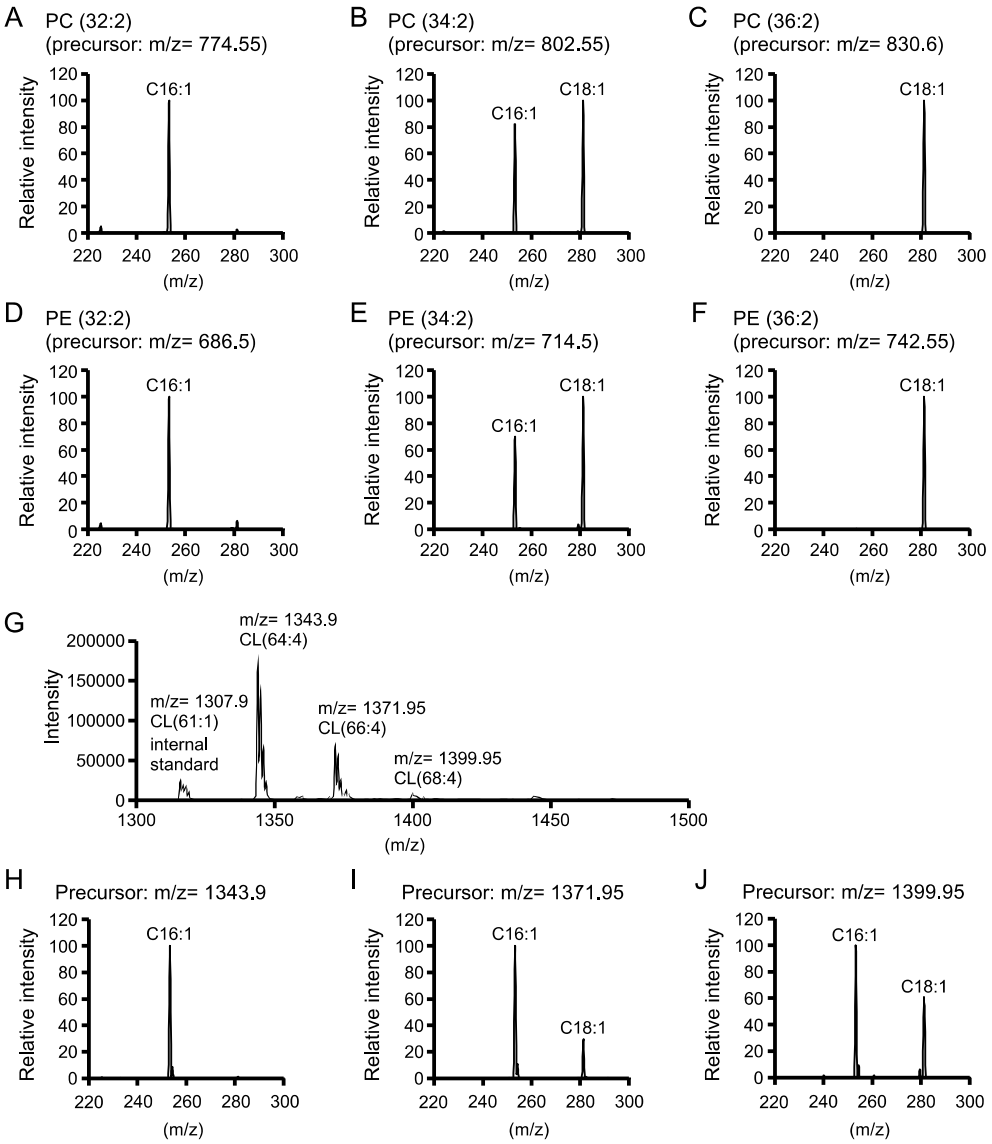

Figure S5. Fatty acid composition of phospholipid molecules in S2 cells. Related to **Figure 5.** Phospholipid molecules were presented in the format PC (X:Y), PE (X:Y), and CL (X:Y), where X denotes the total number of acyl chain carbons and Y denotes the total number of double bonds in acyl chains. Components of fatty acids in PC (32:2) (A), PC (34:2) (B), PC (36:2) (C), PE (32:2) (D), PE (34:2) (E), and PE (36:2) (F) of the crude mitochondrial fraction in S2 cells were analyzed using product ion scan analysis with liquid chromatography with LC-MS/MS. (G) Mass spectra of CL ions ($[M - H]^-$) of S2 cells obtained using liquid chromatography–electron spray ionization–mass spectroscopy (LC-ESI-MS) analysis. Components of fatty acids in CL (64:4) (H), CL (66:4) (I), and CL (68:4) (J) of the crude mitochondrial fraction were also analyzed using product ion scan analysis with LC-MS/MS.

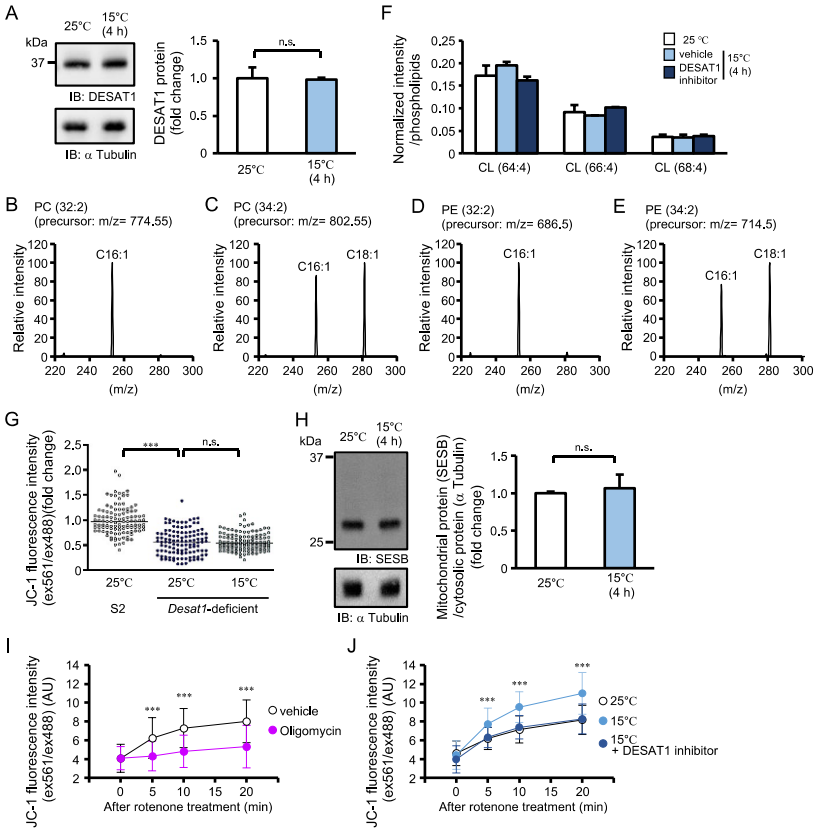

Figure S6. Cold-induced activation of mitochondrial respiration via the DESAT1-dependent regulation of mitochondrial phospholipids. Related to **Figure 6.**

(A) The expression level of DESAT1 protein in S2 cells cultured at 25°C or 15°C for 4h. The amount of DESAT1 protein was normalized with that of α Tubulin. The levels of DESAT1 proteins are shown relative to the amount of DESAT1 protein in cells incubated at 25ºC. Mean ± SD (n = 3). Phospholipid molecules were presented in the format PC (X:Y), PE (X:Y), and CL (X:Y), where X denotes the total number of acyl chain carbons and Y denotes the total number of double bonds in acyl chains. The components of fatty acids in PC (32:2) (B), PC (34:2) (C), PE (32:2) (D), and PE (34:2) (E) of the crude mitochondrial fraction in S2 cells cultured at 15°C for 4h were analyzed using product ion scan analysis with LC-MS/MS. (F) CL molecules in S2 cells treated with or without the DESAT1 inhibitor (1 μM) for 4 h at 25ºC or 15ºC were analyzed using LC-MS/MS. Mean ± SD (n = 3). (G) The mitochondrial membrane potential evaluated by JC-1in wild-type S2 cells or *Desat1*-deficient cells cultured at 25°C or 15°C for 4h. The average value in each cell was plotted. The medians are shown as lines. (H) The amount of mitochondria in S2 cells cultured at 25°C or 15°C for 4h. The amount of a mitochondrial protein SESB was normalized with that of α Tubulin. The levels of SESB proteins are shown relative to the amount of SESB protein in S2 cells incubated at 25ºC. Mean ± SD (n = 3). (I) The proton gradient formation dynamics of S2 cells in the presence (0 min, n = 88; 5 min, n = 88; 10 min, n = 90; 20 min, n = 83) or absence (0 min, n = 82; 5 min, n = 83; 10 min, n = 85; 20 min, n = 86) of oligomycin (3 μM) at 25ºC. (J) The proton gradient formation dynamics of S2 cells cultured at 25ºC for 4 h (0 min, n = 75; 5 min, n = 81; 10 min, n = 88; 20 min, n = 91) and S2 cells treated with (0 min, n = 79; 5 min, n = 89; 10 min, n = 86; 20 min, n = 89) or without (0 min, n = 76; 5 min, n = 81; 10 min, n = 86; 20 min, n = 87) the DESAT1 inhibitor (1 μM) for 4 h at 15ºC. ***P < 0.001. n.s., not significant.

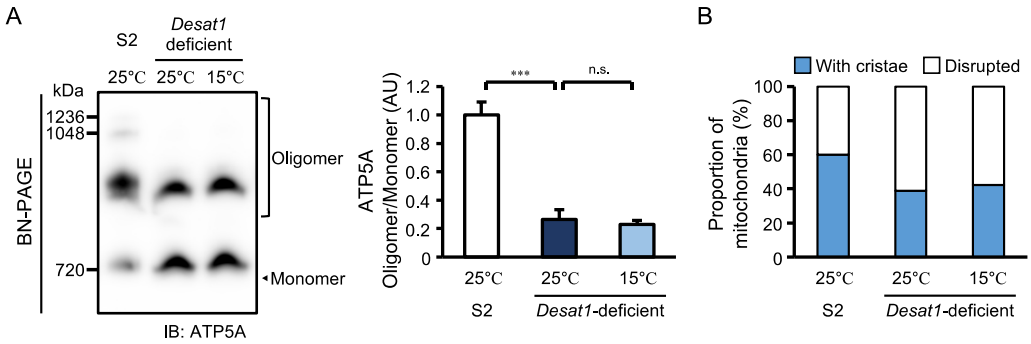

Figure S7. The F_1F_o-ATPase complex and mitochondrial cristae structure during cold exposure in *Desat1*-deficient cells. Related to **Figure 7.**

Wild-type S2 cells or *Desat1*-deficient cells were incubated at 25 ºC or 15 ºC for 4 h. (A) Oligomer formation of F_1F_o-ATPase complex was analyzed using blue native PAGE. The levels of F_1F_o-ATPase oligomer are shown relative to the amount of F_1F_o-ATPase monomer. Mean ± SD (n = 3). ***P < 0.001. n.s., not significant. (B) Based on inner mitochondrial membrane (IMM) structures, mitochondria were classified into two group: “with cristae” and “disrupted”. The proportions of mitochondria classified as Figure 4C in wild-type S2 cells cultured at 25ºC for 4 h (n = 195), *Desat1*-deficient cells cultured at 25ºC for 4 h (n = 162), and *Desat1*-deficient cells at 15ºC for 4 h (n = 165).